

Improving the reliability of pressure ulcer prevention by sensing human bio-signals

Analysis of using piezoelectric sensors to sense respiration and heart rate

J.S. Tijhuis
J.R.H.R. Smit



Improving the reliability of pressure ulcer prevention by sensing human bio-signals

Analysis of using piezoelectric sensors to sense respiration and heart rate

by

J.S. Tijhuis
J.R.H.R. Smit

to obtain the degree of Bachelor of Science
at the Delft University of Technology.

Student number:	4275756, 4217527
Project duration:	April 23, 2018 – July 6, 2018
Thesis committee:	Dr. S.D. Cotofana, TU Delft, chairman
	Prof. dr. P.J. French, TU Delft, supervisor
	Dr. M. Mastrangeli, TU Delft, supervisor
	Dr. MSc D. Cavallo TU Delft
	D. Eldering, Momo Medical

This thesis is confidential and cannot be made public until July 4, 2023.

Abstract

Pressure ulcers, also known as bedsores, are wounds that form when a person sits or lays in the same posture for an extended period of time. Continued pressure being applied to the same spot causes the skin to decay, possibly continuing into underlying tissue if the wounds are not treated. A common and proven practice to prevent pressure ulcers from forming is to regularly change the posture of the patient, so that there is not too much pressure on any one part of the skin.

Momo Medical is creating a sensor system to assist in preventing pressure ulcers. They already have a prototype using force-sensing resistor (FSR) and piezoelectric sensors to measure changes in posture of the patient. The prototype is able to detect if a patient has moved enough, whether on their own or by the nurses, to prevent pressure ulcers. The prototype works, but they need their system to be more reliable.

The research in this thesis focuses on improving the piezoelectric sensors. Momo Medical uses the piezoelectric sensors to measure human bio-signals, mainly respiration and heart rate, through the mattress. Two different printed circuit boards (PCBs) were designed as test set-ups to be able to easily modify the amplifier to measure the piezoelectric sensors separately. Using these test set-ups two common piezoelectric sensors were compared, namely lead zirconate titanate (PZT) and polyvinylidene difluoride (PVDF) sensors. From this comparison it was concluded that the PVDF sensors consistently have a better signal-to-noise ratio (SNR), but that both the PZT and PVDF sensors were able to measure human bio-signals effectively. The PVDF sensors did showed even more promising results when using them in a different mechanical configuration.

In the test set-up the amplifier was also changed to improve the read-out of the sensors. Multiple iterations on the amplifier design were tested. In the final design a non-inverting amplifier was chosen to decouple the amplification from the input impedance of the amplifier and a input impedance of 100M Ω was chosen. Because of the high input impedance in the final design the signal was dampened less and less amplification was needed, thus reducing noise.

Contents

1	Introduction	1
1.1	Pressure Ulcers and Momo Medical	1
1.2	System overview	1
1.2.1	Functional description	1
1.2.2	Patient detection	1
1.2.3	Reposition detection	4
1.3	Project overview	4
1.3.1	Division of subgroups and tasks	4
1.3.2	Scrum	4
1.4	Problem definition	4
2	State of the art analysis	7
2.1	Analysis of available sensors	7
2.1.1	Piezoceramic sensors	7
2.1.2	Piezoelectric thin film	8
2.1.3	Model of a piezoelectric sensor	8
2.2	Analysis of the circuit of Momo Medical	10
2.2.1	Amplifier topology	10
2.2.2	ADC stage	10
3	Development of test setup	13
3.1	Design of the amplifier	13
3.1.1	Amplifier topology	13
3.1.2	Operational amplifier selection.	18
3.2	Design of the ADC stage.	19
3.3	Design of the power stage	20
3.4	Shielding	20
3.5	Mechanical setup of the sensor	20
3.6	PCB layout	24
4	Results	25
4.1	Determining bandwidth of human bio-signals	25
4.2	Comparing different sensors	25
4.2.1	Existing sensor system with PZT	25
4.2.2	Comparing PZT and PVDF sensors with first iteration test set-up	26
4.2.3	Comparing PZT and PVDF sensors with second iteration test set-up	26
5	Discussion	29
5.1	Future work	29
6	Conclusions	31
6.1	Recommendations	31
A	Measurement data	33
B	Matlab scripts	35
C	Printed circuit board design	41

Introduction

1.1. Pressure Ulcers and Momo Medical

Pressure ulcers develop when skin is subjected to a mechanical load over time, resulting in tissue damage [?]. Within a wide range of patients pressure ulcers occur, often accompanied by severe pain. This is resulting in a prolonged hospital stay [?]. The costs of this prolonged stay in the Netherlands varies from around \$500 million, approximately 1.2% of total health care costs in the Netherlands (based on the low estimations), to around \$2 billion, or approximately 6.6% of the Netherlands total health care costs (based on the high estimations) [?]. The pressure ulcers are classified in 4 stages. In stage 1 the area gets painful and with dark skin tones. Stage 2 is where the skin partially suffers from thickness. In stage 3 the skin has lost the full thickness. Lastly in stage 4 there patient suffers from full tissue thickness loss and bone becomes visible [?].

The company Momo Medical is developing a sensor plate with the goal of preventing pressure ulcers by using sensor data attained from the patient laying on his bed to guide the nurses, whom are responsible for re-positioning the patients [?]. The sensor plate is placed between the mattress and the frame and has sensors to detect the dynamic and static behaviour of the patient. This data is processed by an algorithm to determine the position of the patient and how long the patient has remained in the same position.

1.2. System overview

The complete system consists of a sensor plate and a control box. The plate contains eleven sensors: two PZTs piezoceramic disks to measure dynamic forces such as respiration and heart rate, eight FSRs to measure absolute weight distribution across the plate and one accelerometer to measure the angle of a hospital bed. A schematic overview is shown in figure 1.1.

Figure 1.2 shows an exploded view of the sensor plate. Figure 1.3 provides insight of the positioning of the plate and its sensors relative to the mattress and the patient.

1.2.1. Functional description

When a patient lies down on the mattress, a timer starts inside the control box. This timer stops when the patient has left the bed and resets when the patient did a major change in position, namely from side to back or to a face-down position (or vice versa). When the timer reaches three hours, the nurse will be alerted and the patient must be repositioned to avoid the development of a pressure ulcer. The sensor plate is currently only placed under patients with a high risk on pressure ulcers.

1.2.2. Patient detection

To detect if there is a patient lying on a bed, the data from the PZTs is used, since these sensors sense human bio-signals like respiration and ballistocardiography (BCG). The change in the PZT outputs will be higher due to these physical signals. The algorithm assumes a patient is present when the standard deviation of the data reaches a certain threshold.

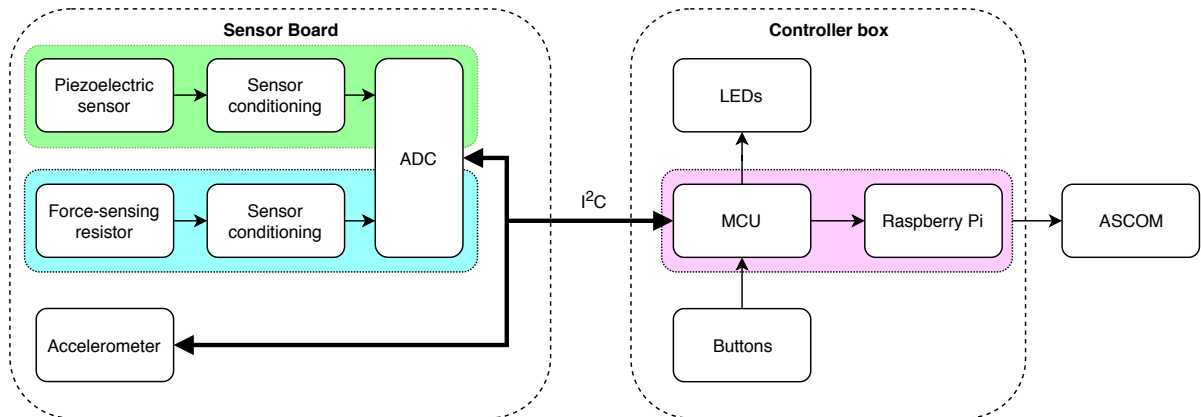


Figure 1.1: Schematic overview of the system. The green area indicates the focus of team PZT, the blue area the focus of team FSR, the pink area the focus of team microcontroller unit (MCU).

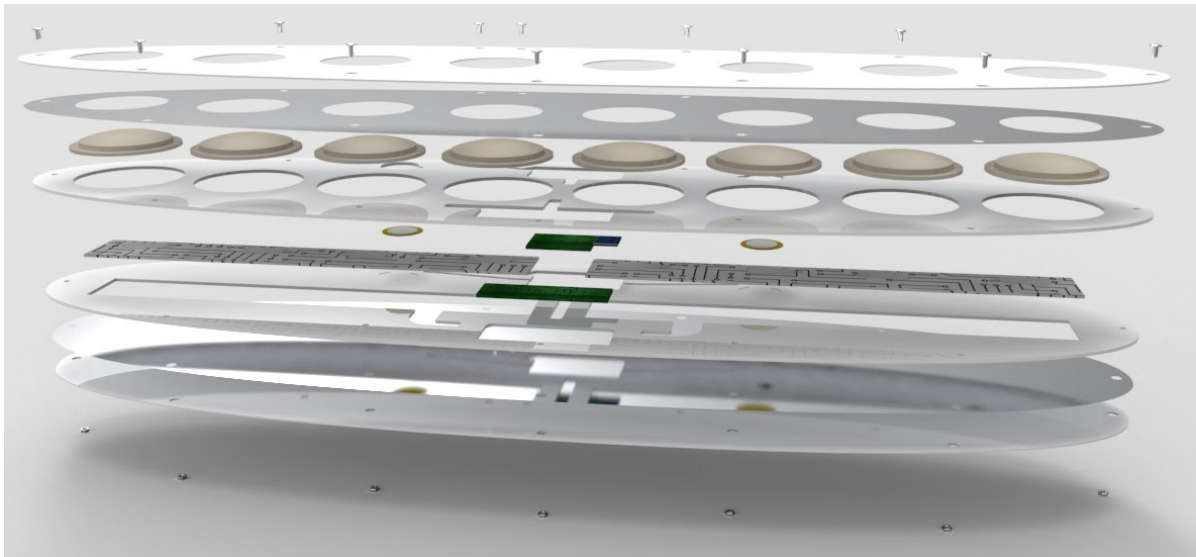


Figure 1.2: An exploded view of the sensor plate

Source: Kwinten van Buuren, Momo Medical 2018

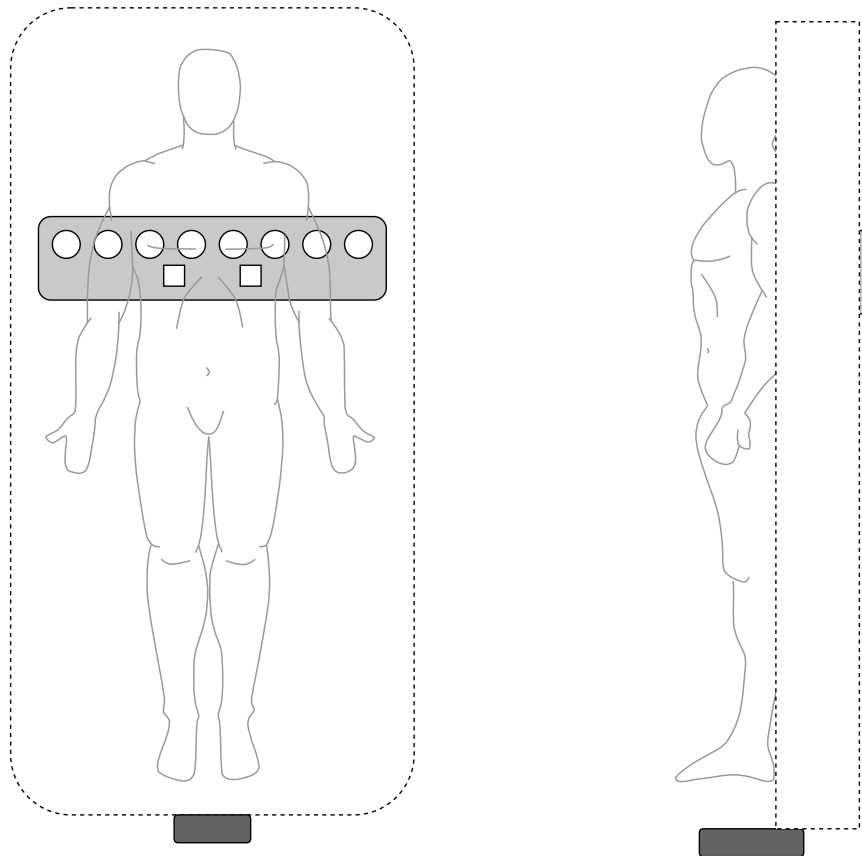


Figure 1.3: Indication of position of the plate, sensors and control box. The dashed line indicates the mattress, the dark grey rectangle is the control box, the light grey rectangle is the sensor plate, the white circles indicate the FSRs and the white squares indicate the piezoceramic disks. Note that this overview is not perfectly to scale.

Source: Own work

1.2.3. Reposition detection

As figure 1.3 shows, the FSRs are spread out over the width of the bed. Every FSR measures the static force on a particular area of the bed. The difference in output over time of every sensor is observed. When the sum of these absolute values reaches more than a certain threshold, the algorithm detects a major movement.

1.3. Project overview

At the moment the output of the sensors on the sensor plate is not reliable enough, and therefore Momo Medical cannot begin the production of the sensor plate yet. This Bachelor Graduation Project (BAP) group contains 6 individuals and has been established to increase the reliability of Momo Medical's system.

1.3.1. Division of subgroups and tasks

The BAP-group has been divided into 3 subgroups of 2 members each. The different colours in figure 1.1 view of the division of the subgroups in relation to the system. The first subgroup (team FSR) focuses on the FSRs, the second group (team PZT) on the piezoelectric sensors and lastly the third group (team MCU) on the MCU and a part of the algorithm. Each member has also been given an additional task, for which this person is responsible for during the entire project. The division of subgroups and tasks are as follows:

- Jordy Langereis - team FSR - chairman
- Duco Veldhuijzen - team FSR - responsible for Ethics essay
- Jasper Smit - team PZT - minutes secretary
- Job Tijhuis - team PZT - responsible for external contact
- Tu Hoang - team MCU - responsible for Business-plan
- Joep Dumont - team MCU - scrum master

1.3.2. Scrum

While working on the different projects, Scrum is used to iteratively work towards a final product. Scrum is a framework where the order of processes is defined in an agile way. Figure 1.4 gives a simplified overview of scrumming.

A period of two weeks has been defined as a 'sprint', where at the start of every sprint a sprint planning is made. In this sprint planning the teams divide and order tasks that are required to deliver a prototype at the end of the sprint. During the sprint at the start of every day every member tells what he has done the previous day, what he will do this present day and what their current obstacle is; this is called a stand-up. At the end of the sprint the previous 2 weeks are reviewed in a retrospective. In the next sprint the suggestions from the retrospective are applied and a new sprint planning is performed. This type of project flow ensures that the product can change a lot based on the experience and feedback that has been gained while working on the product itself. Instead of delivering one product at the end of the project, the product has been presented a number of times and therefore improved during the project. The Scrum master monitors and helps the team on a daily basis to make sure that Scrum is performed correctly.

1.4. Problem definition

As stated before, the focus of this subgroup lies on the piezoelectric sensors. The sensors are currently only used to detect if a patient is present, but the data is not used for anything else. This is partly due to the algorithm not being fully developed and partly due to the quality of the signals received.

The main focus of this thesis will be making the detection of human bio-signals from the patient received by the piezoelectric sensors more reliable, to assist in detecting the posture of the patient.

Problems identified via the algorithm group of R&D were mostly the long-term clipping of the sensor, paralysing the algorithm for a while.

The problem is very broad, so it is important to clearly state the scope of the problem. This thesis will mainly focus on developing a test setup, comparing piezo thin-film sensors to piezoceramic sensors, comparing different piezo thin-film sensors, and characterising the human bio-signals.

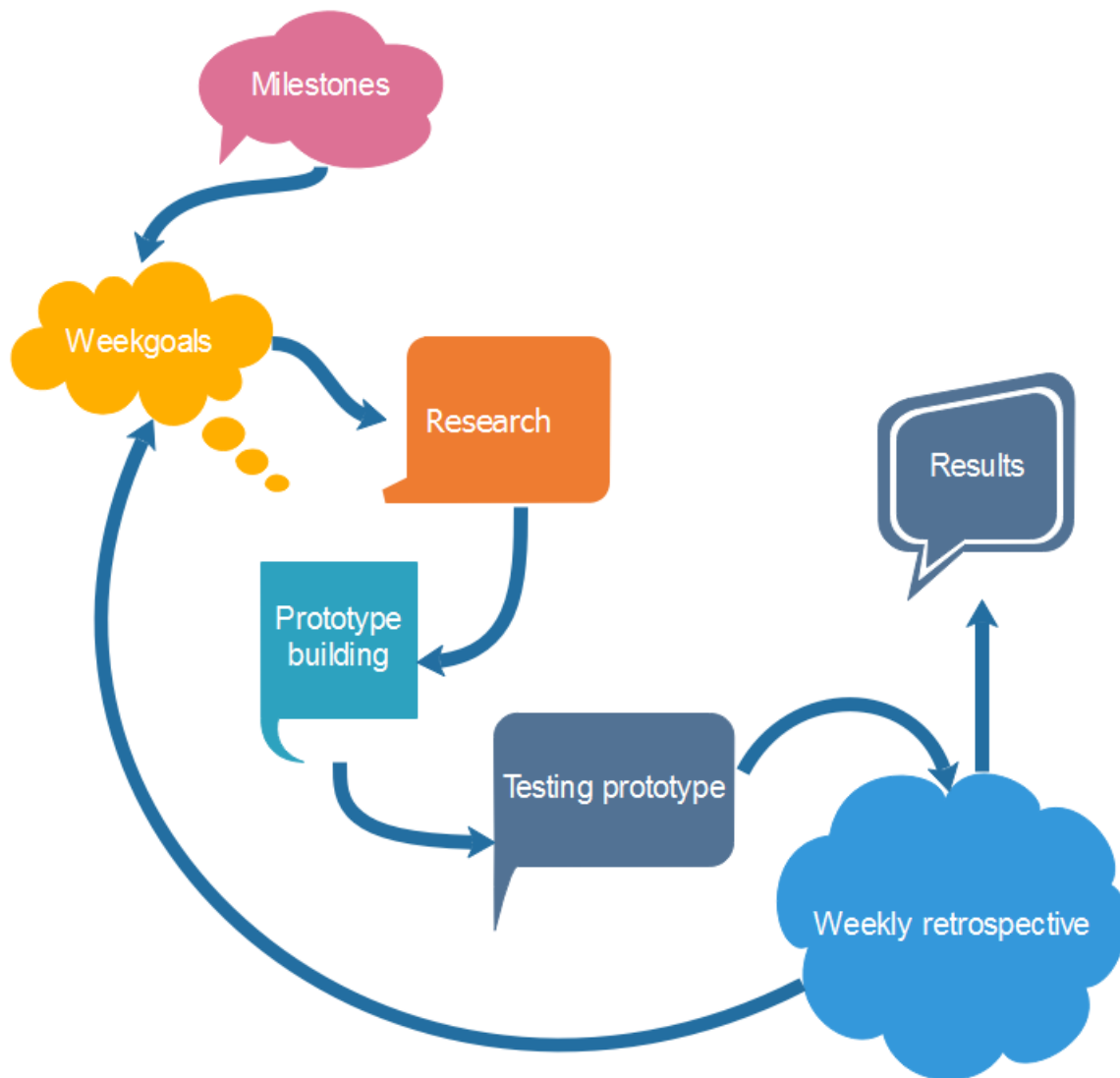


Figure 1.4: A simplified overview of Scrumming.

Source: Thomas Bakker, Momo Medical 2017

2

State of the art analysis

2.1. Analysis of available sensors

From the literature study into piezoelectric sensors it was found that there are a couple of different piezoelectric sensors that were already being used in measuring heartbeat and respiration signals. The main requirements for the sensors are that they are sensitive enough and also do not pick up too much interference from movement happening around the bed. The requirement to reduce interference came from Momo Medical, because this is a problem they have in their current piezoelectric sensors.

2.1.1. Piezoceramic sensors

The sensor that Momo Medical currently uses is a piezoceramic sensor. The most common piezoceramic material used in piezoelectric elements is PZT, this is also the case in the current sensor plate of Momo Medical. Advantages of PZT are that it is cheap to produce and has good piezoelectric properties compared to other piezoceramic materials. PZT has already been used in many applications and has good piezoelectric properties [?], because of this PZT is the piezoceramic that was used in comparing different sensor types. PZT sensors have been used in the study [?], where piezoceramic were placed between the floor and the bed and respiration and heart beat was measured.

The type of PZT sensor that was used was a round thin metallic plate, brass in this case, with the ceramic material deposited on part of the plate. Figure 2.1 shows a schematic representation of the sensor. These sensors are bought with leads already attached.

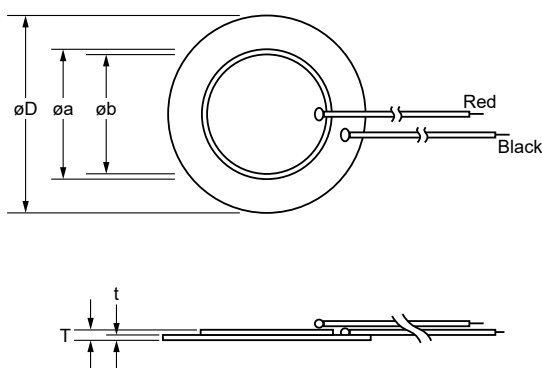


Figure 2.1: Schematic representation of a PZT sensor. Image from: <https://www.murata.com/products/sound/sounder#catalog>, accessed June 2018.

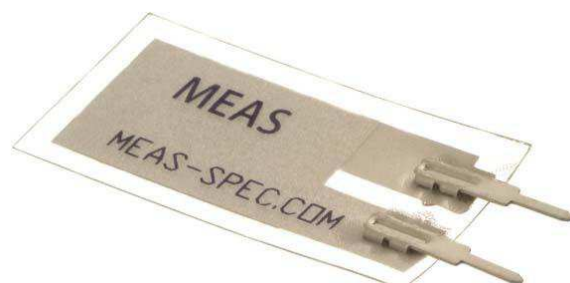


Figure 2.2: PVDF sensor. Image from: <http://www.te.com/usa-en/product-CAT-PFS0006.html>, accessed June 2018.

2.1.2. Piezoelectric thin film

Another form of piezoelectric sensors are piezoelectric thin film sensors. The most common material used in piezoelectric thin films is PVDF, which has very good piezoelectric properties [?]. From the literature study it was quite clear that PVDF sensors have a lot of potential and that is very suited to medical applications, especially sensing human bio-signals [?].

The PVDF sensor used was a thin film sensor of 1cm by 2cm as seen in figure 2.2. It is a flexible sensor that can bend and will quickly return to being flat when no force is present. These sensors are bought from TE connectivity [?].

2.1.3. Model of a piezoelectric sensor

A piezoelectric sensor can be modeled as in figure 2.3 [?]. In this model, the value of the voltage source V_p is given by eq. 2.1, where q_p depends on the piezoelectric constant of the sensor. R_p amounts for the discharging of C_p , and is very large ($>1G\Omega$). For both the PZT and the PVDF sensor, the impedance is unknown. The PZT sensors were bought from AliExpress (China) and a datasheet was not provided. The PVDF sensor did have a datasheet, but nothing was explicitly stated about the impedance of the sensor [?]. However, plots in the datasheet are made for a sensor with an impedance of 480pF.

$$V_p = \frac{q_p}{C_p} \quad (2.1)$$

To measure C_p , the sensors were placed in a low-pass RC configuration (see figure 2.4). On the low-pass filter, a 5V sine wave was applied, and the frequency was increased until the peak-to-peak voltage dropped to 3.53V ($= \frac{1}{\sqrt{2}} \cdot 5V$), which is the cutoff frequency. The magnitude response of the entire system including the output impedance of the signal generator (50Ω) and the input impedance of the oscilloscope ($1M\Omega$) (eq. 2.2) can be rewritten to extract the capacitance (eq. 2.3). The input and output impedances have been modelled in figure 2.6. Scripts B.1 and B.2 were used for these calculations.

At 50Hz both sensors showed $5.00V_{pp}$ on the oscilloscope. The signal generation and measurement was done using a Rigol MSO1074 oscilloscope. The measurement was done with eleven sensors of each type.

For the PZT sensors C_p averaged at 22.4nF with a standard deviation of 1.25nF (5.6%) with a maximum deviation of 1.9nF (8.4%). For the PVDF sensors C_p averaged at 508pF, which was close to the 480pF unexplicitly stated in the datasheet [?]. The standard deviation of the PVDF sensor was 17.8pF (3.5%) with a maximum deviation of 32pF (6.3%). For the measured frequencies and corresponding capacitance see table A.1 and A.2 in appendix A. The resulting models are displayed in figure 2.5 and will be used in this report.

$$\left| \frac{V_{out}}{V_{in}} \right|^2 = \left| \frac{1}{1 + \frac{R_1 + R_{sg}}{R_{osc}} + j2\pi f_{-3dB} C_p (R_1 + R_{sg})} \right|^2 \quad (2.2)$$

$$C_p = \frac{\sqrt{2 - \left(1 + \frac{R_1 + R_{sg}}{R_{osc}}\right)^2}}{2\pi f_{-3dB} (R_1 + R_{sg})} \quad (2.3)$$

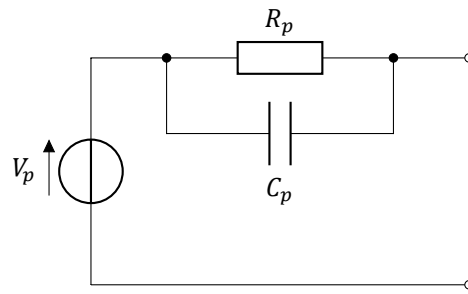


Figure 2.3: A model of a piezoelectric sensor.

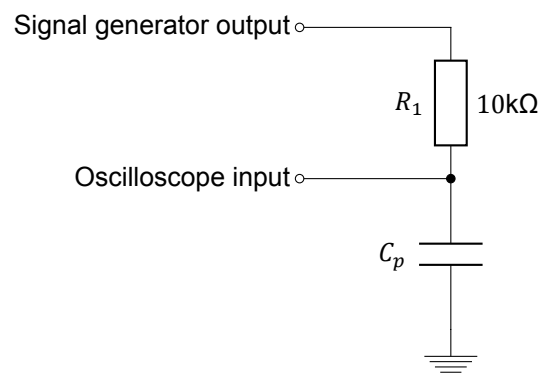
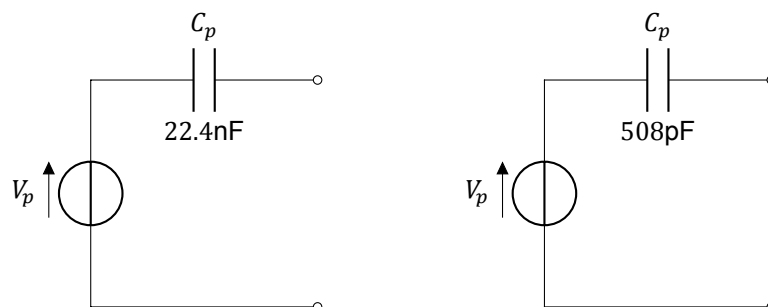
Figure 2.4: The measurement setup for the capacitance of the sensors. C_p is the sensor being measured. R is a $10\text{k}\Omega$ 1% tolerance resistor, placed in series with the sensor to create a low-pass filter.

Figure 2.5: Models of piezoelectric sensors. On the left a model of a PZT sensor, on the right a model of a PVDF sensor.

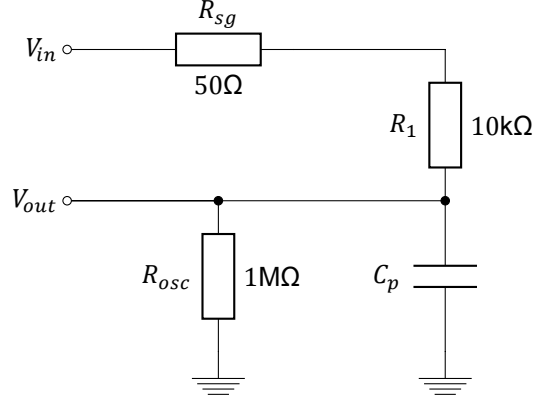


Figure 2.6: The model of the measurement setup for the capacitance of the sensors. C_p is the sensor being measured. R_1 is a 10kΩ 1% tolerance resistor, placed in series with the sensor to create a low-pass filter. The output impedance of the signal generator (50Ω) and the input impedance of the oscilloscope (1MΩ) have been modelled by R_{sg} and R_{osc} . The corresponding transfer function is given by eq. 2.2.

2.2. Analysis of the circuit of Momo Medical

2.2.1. Amplifier topology

The topology Momo Medical currently uses is a charge amplifier. The charge amplifier consists of two resistors, a capacitor and an operational amplifier, as seen in figure 2.7. The amplifier also features a low-pass filter at the output. The input impedance is 820kΩ and the low-pass filter at the output has a cutoff frequency at $f_{-3dB} = 11.3\text{Hz}$. The charge amplifier itself also has a low-pass filter characteristic (C_1 and R_2) with a cutoff-frequency at $f_{-3dB} = 10.3\text{Hz}$.

The transfer function of this model acting on the circuit of Momo Medical is given by eq. 2.4 using the output voltage as the input, and plotted in figure 2.8 using script B.3. When using the charge q as the input, the transfer function becomes eq. 2.5, and is plotted in figure 2.9. The responses in these figures of the PZT and PVDF cannot be directly compared, as the charge and voltage produced at a certain force might not be the same due to the mechanical properties of the sensor and the setup.

$$\frac{V_{out}}{V_{in}} = -\frac{1}{\left(\frac{1}{R_2} + sC_1\right)\left(R_1 + \frac{1}{sC_p}\right)} \cdot \frac{1}{sC_2R_3 + 1} \quad (2.4)$$

$$\frac{V_{out}}{q} = -\frac{1}{C_p} \cdot \frac{1}{\left(\frac{1}{R_2} + sC_1\right)\left(R_1 + \frac{1}{sC_p}\right)} \cdot \frac{1}{sC_2R_3 + 1} \quad (2.5)$$

This response is sub-optimal because the gain at 0.5Hz, which is around the respiration frequency, is 23dB while the peak amplification is around 7Hz with 42dB.

2.2.2. ADC stage

Momo Medical uses a high performance ADC, the ADS1115 [?]. The ADS1115 is a 16-bit 860 samples/s ADC with an I²C bus interface. At a range of 5V, the least-significant bit (LSB) of the ADS1115 signifies 76μV. At 860 samples/s the highest frequency signal measurable will be 430Hz (Nyquist frequency).

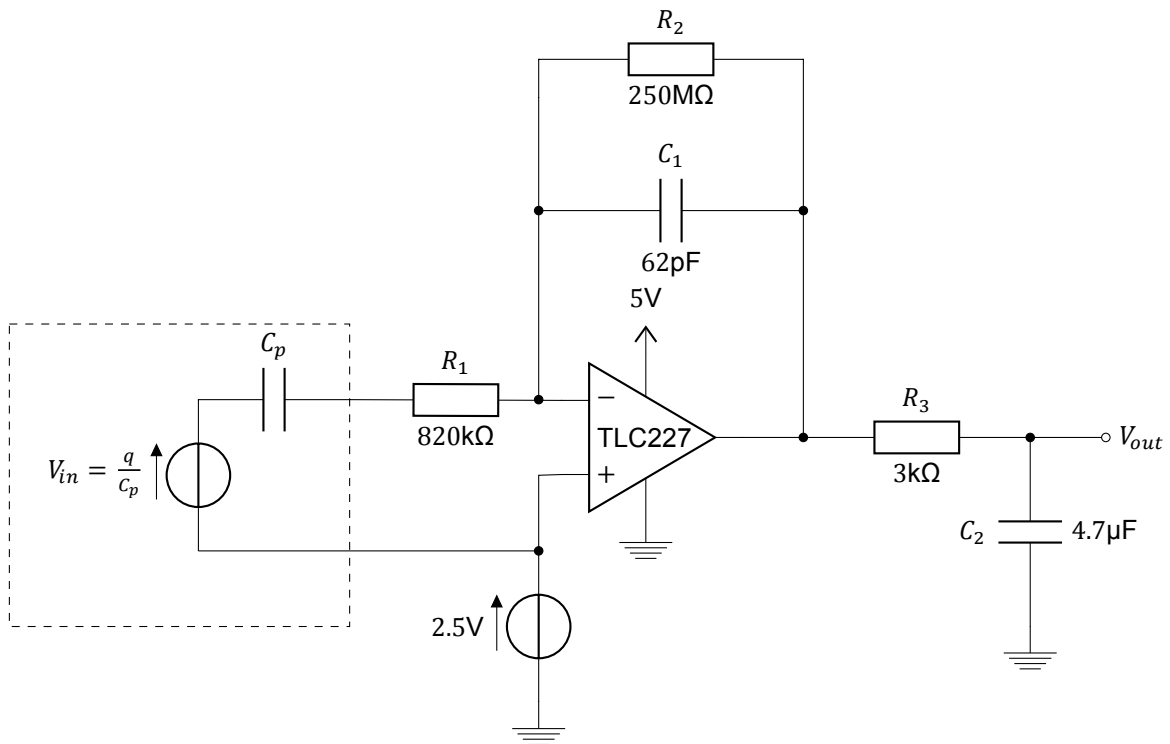


Figure 2.7: The schematic of the sensor conditioning circuit currently used by Momo Medical. The dashed box is the model of the piezoelectric sensor.

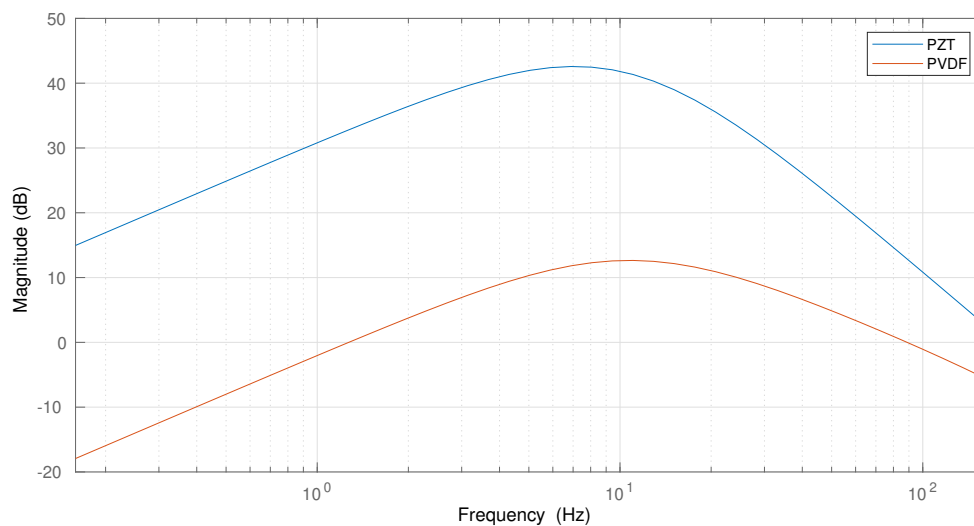


Figure 2.8: Frequency response of the sensor conditioning circuit used by Momo Medical for both the model of the PZT and PVDF sensor. The circuit features two low-pass and one parasitic high-pass filter.

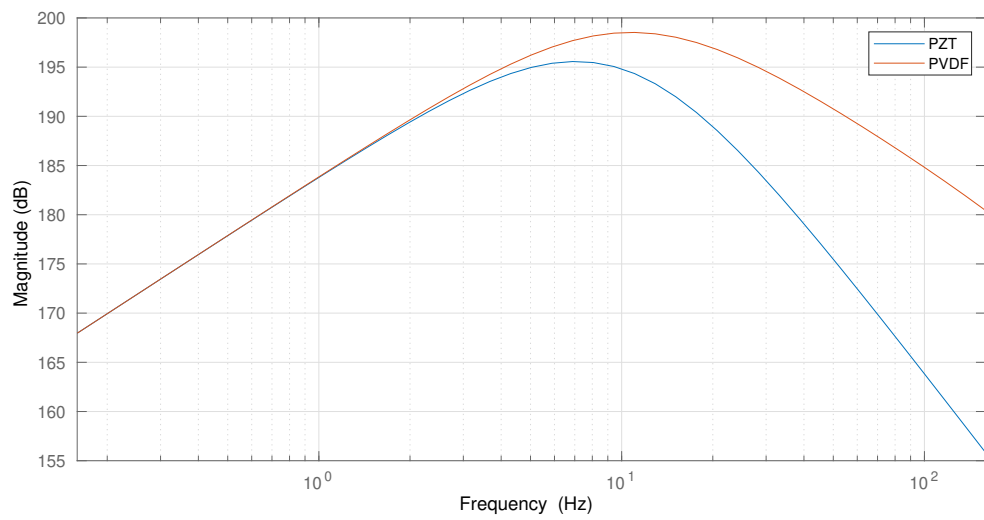


Figure 2.9: Frequency response of the sensor conditioning circuit used by Momo Medical for both the model of the PZT and PVDF sensor. The circuit features two low-pass and one parasitic high-pass filter.

3

Development of test setup

Rather than testing, modifying and swapping out sensors in a sensor plate of Momo Medical, a dedicated PCB for testing was developed. This chapter describes the design choices made during the development of this test setup.

The goal for this test setup was to provide a simple dedicated system used for reading and comparing piezoelectric sensors.

The focus on the first iteration of the test board was to make it easier to swap out the sensors and modify the amplifier. In the design of the PCB, the sensor was kept unisolated but other measures were taken to reduce noise to a minimum. In the second iteration of the test board the amplifier was redesigned and the sensor was completely shielded to obtain a reference signal.

3.1. Design of the amplifier

The first iteration of the amplifier was designed to match the amplifier currently used by Momo Medical (see figure 2.7). A lot of extra parts were added in the schematic but not populated on the board for possible changes to the amplifier in the future.

3.1.1. Amplifier topology

First iteration of amplifier topology

A charge amplifier is used to measure quasi-static signals on piezoelectric sensors and to remove the effect of the capacitance of the cable of the piezoelectric sensor. Currently at Momo Medical these cables are 80mm and 100mm long.

In the new design, however, the cables are removed from the sensors to minimize noise. This also defeats the purpose for a charge amplifier, so C1 from the schematic from Momo Medical (fig. 2.7) was removed and the circuit became a simple inverting amplifier as seen in figure 3.3.

In the charge amplifier and the first iteration of the new design, the input impedance is set by R_1 , but the gain is also dependent on R_1 . R_1 cannot be decreased, as the signal-to-noise ratio would drop and the cutoff frequency of the RC filter with the internal capacitance C_p would rise, and it cannot be increased, as R_2 scales linearly with R_1 to keep the same gain it would hit the limits of available resistor values.

R_2 was set to 500M Ω instead of 250M Ω to increase the gain, while keeping the input impedance, R_1 , the same. Also the RC filter at the output has been redesigned with different component values, selecting a cheaper and more available capacitor of 150nF instead of 4.7 μ F. The cutoff frequency was unchanged at 10Hz.

The transfer function with the voltage as input is given by eq. 3.1, the corresponding frequency response can be seen in figure 3.1. The transfer function with the charge as input is given by eq. 3.2, the corresponding frequency response can be seen in figure 3.2. The responses in these figures of the PZT and PVDF cannot be directly compared, as the charge produced at a certain force might not be the same due to the mechanical properties of the sensor and the setup. When looking at these responses, the effect of removing the feedback capacitor can be seen by the fact that frequencies above 10Hz are way less attenuated than in the charge amplifier. The PVDF has especially more high frequency

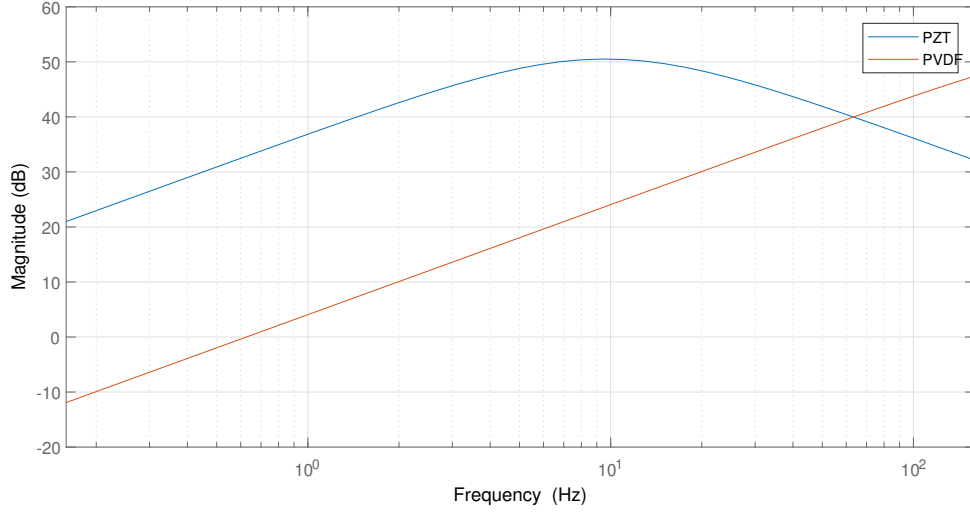


Figure 3.1: Frequency response of the first iteration of the development board, using the voltage source in the model as the input. The circuit features a low-pass filter with a cutoff frequency at 106Hz. The responses of the PZT and PVDF cannot be directly compared, as the voltage produced at a certain force might not be the same due to the mechanical properties of the sensor and the setup. This plot was generated with script B.4.

components due to the high-pass cutoff frequency being at 382Hz, so this set-up is less suited for the PVDF.

$$\frac{V_{out}}{V_{in}} = -\frac{sR_2C_p}{sR_1C_p + 1} \cdot \frac{1}{sC_1R_3} \quad (3.1)$$

$$\frac{V_{out}}{V_{in}} = \frac{1}{C_p} \cdot -\frac{sR_2C_p}{sR_1C_p + 1} \cdot \frac{1}{sC_1R_3} \quad (3.2)$$

Second iteration of amplifier topology

To be able to increase the gain orthogonally with the input impedance, a non-inverting amplifier was selected as the topology for the second iteration, as seen in figure 3.6.

The input impedance of the non-inverting amplifier can be set with R_1 , to a maximum equal to the input impedance of the operational amplifier (op-amp) (by removing R_1). The gain is set by different resistors (R_2 and R_3) than the resistor that determines the input impedance.

R_1 does however have a secondary function, it must also discharge the internal capacitance of the piezoelectric sensor. With an input impedance of 100M Ω the RC time will be 2.2s for the PZT sensor and 51ms for the PVDF sensor. This was no problem with the non-inverting amplifier where the RC time is 18ms for the PZT sensor and 417 μ s for the PVDF sensor.

The cutoff frequency of the internal high-pass filter will be at $f_{-3dB} = 71$ mHz for the PZT and 3.1Hz for the PVDF. The transfer function with the voltage as input is given by eq. 3.3, the corresponding frequency response can be seen in figure 3.4. The transfer function with the charge as input is given by eq. 3.4, the corresponding frequency response can be seen in figure 3.5. The responses in these figures of the PZT and PVDF cannot be directly compared, as the charge produced at a certain force might not be the same due to the mechanical properties of the sensor and the setup.

$$\frac{V_{out}}{V_{in}} = \frac{sR_1C_p}{sR_1C_p + 1} \cdot \left(1 + \frac{R_2}{R_3}\right) \cdot \frac{1}{1 + sC_1R_4} \quad (3.3)$$

$$\frac{V_{out}}{q} = \frac{1}{C_p} \cdot \frac{sR_1C_p}{sR_1C_p + 1} \cdot \left(1 + \frac{R_2}{R_3}\right) \cdot \frac{1}{1 + sC_1R_4} \quad (3.4)$$

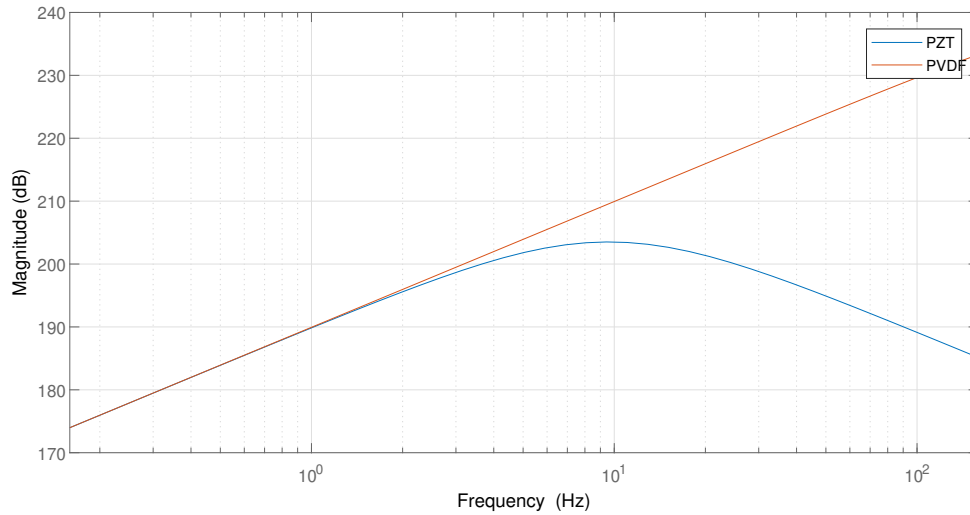


Figure 3.2: Frequency response of the first iteration of the development board, using the charge in the model as the input. The circuit features a low-pass filter with a cutoff frequency at 106Hz. The responses of the PZT and PVDF cannot be directly compared, as the voltage produced at a certain force might not be the same due to the mechanical properties of the sensor and the setup. This plot was generated with script B.4.

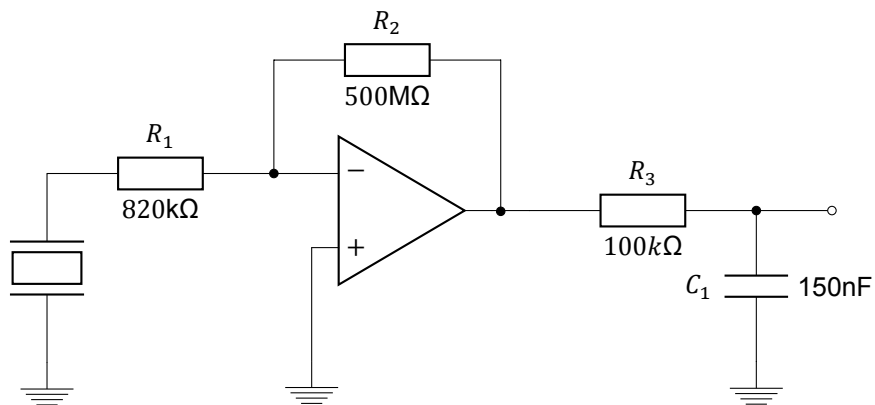


Figure 3.3: The first iteration of the schematic for amplifier for the piezoelectric sensor.

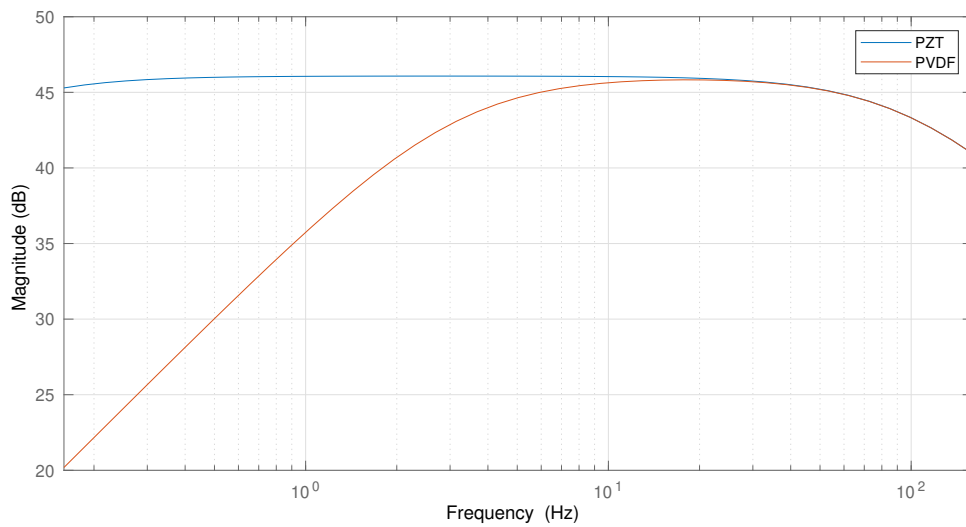


Figure 3.4: Frequency response of the second iteration of the development board, using the voltage source in the model as the input. The circuit features a low-pass filter with a cutoff frequency at 106Hz. The responses of the PZT and PVDF cannot be directly compared, as the voltage produced at a certain force might not be the same due to the mechanical properties of the sensor and the setup. This plot was generated with script B.5.

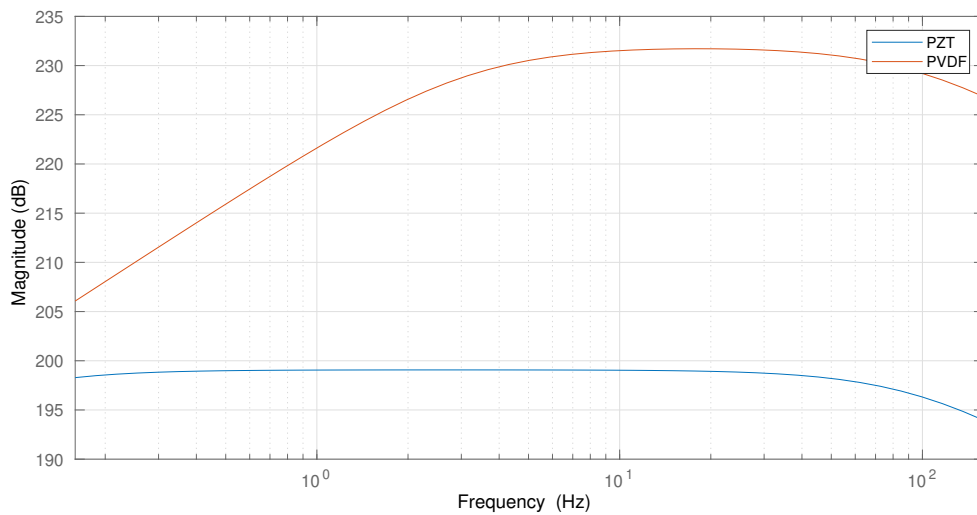


Figure 3.5: Frequency response of the second iteration of the development board, using the charge q in the model as the input. The circuit features a low-pass filter with a cutoff frequency at 106Hz. The responses of the PZT and PVDF cannot be directly compared, as the charge produced at a certain force might not be the same due to the mechanical properties of the sensor and the setup. This plot was generated with script B.5

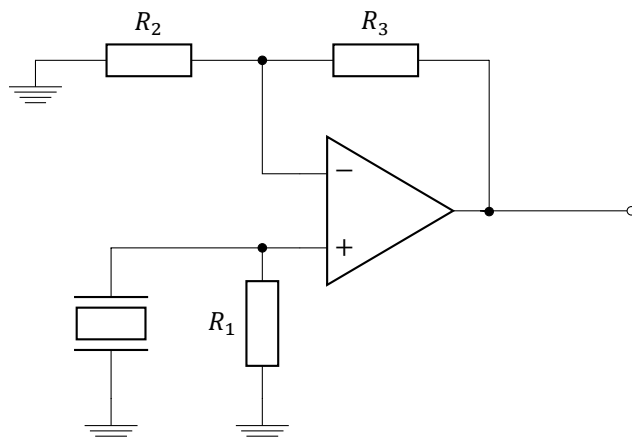


Figure 3.6: The new topology of the amplifier for the piezoelectric sensor. R_1 is used to discharge the internal capacitor of the piezoelectric sensor and determines the input impedance. R_2 and R_3 determine the gain.

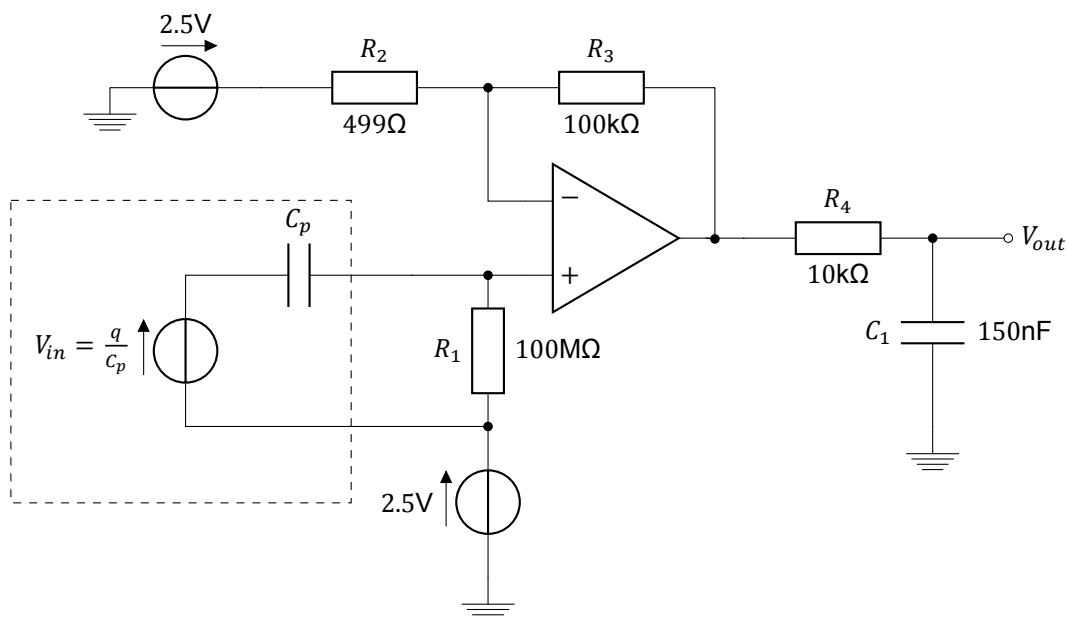


Figure 3.7: The new topology of the amplifier for the piezoelectric sensor. R_1 is used to discharge the internal capacitor of the piezoelectric sensor and determines the input impedance. R_2 and R_3 determine the gain.

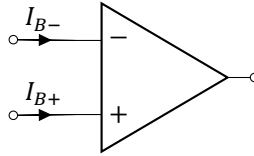


Figure 3.8: Input bias currents in an operational amplifier.

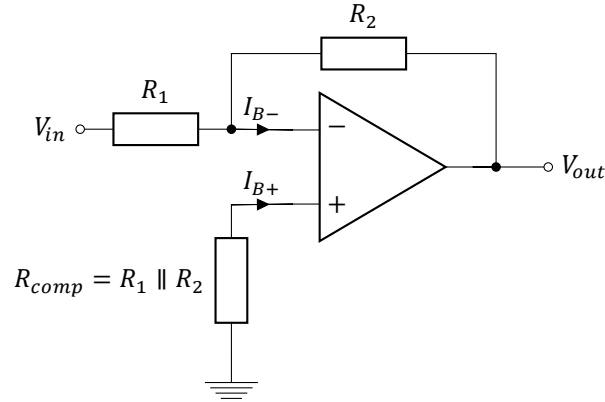


Figure 3.9: Compensation for input bias on an inverting amplifier by matching impedances.

3.1.2. Operational amplifier selection

The amplifier should introduce as less as possible noise and non-linearities to provide optimal results for the test setup. Alternatives to the currently used operational amplifier were considered to discover what could be improved. In the following paragraphs some relevant DC characteristics of op-amps are introduced, all contributing to an offset in the output of the amplifier.

Most AC characteristics like bandwidth and slew-rate are not relevant for this application as the respiration and BCGs signal consist only of low frequencies ($\ll 1\text{kHz}$). Also the drift over temperature is not very relevant, as the temperature in a hospital is regulated. The op-amp itself will not heat up either, as it is not driving anything but the input of the ADC. The only temperature change may come from the patient lying on the bed, but there is a mattress between the patient and the circuit so the temperature change and drift will be minimal.

Input bias and offset current

The input bias current I_B is average of the currents into the inputs of the op-amp [?] (eq. 3.5). The input bias current is unwanted because it produces an offset voltage at the op-amp input, which is specified by eq. 3.6 and is dependent on the source impedance Z_S . This is especially a problem for amplifying piezoelectric sensors, as the source impedance is very high.

$$I_B = \frac{I_{B+} + I_{B-}}{2} \quad (3.5)$$

$$V_B = I_B \cdot Z_S \quad (3.6)$$

This bias at the input can be compensated by matching the impedance at both inputs as seen in figure 3.9. There will, however, still be an offset voltage at the input of the amplifier due to the fact that I_{B-} is not equal to I_{B+} . The difference between the input bias current in the positive input and the input bias current in the negative input is the input offset current [?], see eq. 3.7. The offset in the input voltage resulting from the input offset current in an amplifier with compensated input impedance is given by eq. 3.8.

$$I_{IO} = I_{B-} - I_{B+} \quad (3.7)$$

$$V_{IO} = I_{IO} \cdot Z_S \quad (3.8)$$

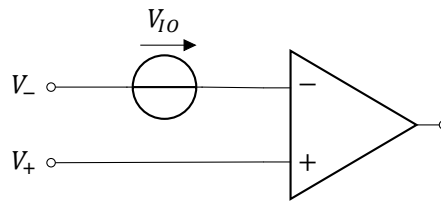


Figure 3.10: Model of the input voltage offset in an operational amplifier.

Table 3.1: Comparison between the TLC227x and the OPAx376. The selected parameters are relevant for reading high source impedance sensors. The typical values are displayed, with the maximum values in parentheses. The price is provided by the website of Texas Instruments, based on the TLC2272 and the OPA376. All parameters are at 25°C

	I_B	I_{IO}	V_{OS}	Price 1ku
TLC227x	1pA (60pA)	0.5pA (60pA)	300μV (2500μV)	0.68\$
OPAx376	0.2pA (10pA)	0.2pA (60pA)	5μV (25μV)	0.65\$

Not only the input bias currents causes an offset in the output voltage, but also the input offset voltage V_{IO} . The op-amp has an input voltage offset because of mismatched input transistors [?]. The effect of the input offset voltage can be modeled as in figure 3.10. Together with the input bias current, the total input offset voltage V_{TIO} can be calculated with eq. 3.9.

$$V_{IO} = I_B \cdot Z_S + V_{IO} \quad (3.9)$$

Comparison between OPAx376 and TLC227x

The OPAx376 precision op-amp was selected as the replacement for the TLC227x. The OPAx376 features lower input bias current, lower input offset voltage against a higher cost [?]. However, as the amplifier should be placed as close to the sensor as possible to minimize noise, it would be preferred to have two individual packages containing one amplifier each. This is not possible with the TLC227x; it only comes in dual (TLC2272) or quad (TLC2274) amplifier configurations [?]. The OPAx376 does have a single amplifier version (OPA376).

An overview of the input offset and bias currents, the input offset voltage and the price can be seen in table 3.1. Taking all parameters into account and using eq. 3.9, the resulting total input offset voltage can be seen in table 3.2. Both the TLC2274 and the OPA376 have an input noise voltage of < 1μA and have not been accounted for in the calculation of the input offset voltage.

3.2. Design of the ADC stage

The resolution and sample frequency of the ADC Momo Medical uses are more than suited for the test setup, which is why it was used in the first iteration of the PCB.

The downside of the ADS1115 is the cost, it costs 2.30USD per kilo unit [?]. There exists a pin compatible alternative, the ADS1015, which is only 1.15USD per kilo unit [?] but features only a 12-bit ADC. It does have a higher sample frequency at 3.3k samples/s. The ADS1015 was placed on two of the three second iteration development boards, as a third was not readily available at the time. The third board featured an ADS1115.

For the I²C bus used to communicate with the ADC, the board featured two pull-up resistors with a value of 4.7kΩ for the serial clock (SCL) and serial data (SDA) lines, and an external power input for the pull-up resistors.

Table 3.2: The total input offset voltage for the TLC227x and the OPAx376 at different source impedances, calculated with eq. 3.9 using typical values and maximum values in parentheses.

	V_{IO} at $Z_S = 1M\Omega$	V_{IO} at $Z_S = 10M\Omega$	V_{IO} at $Z_S = 100M\Omega$
TLC227x	301μV (2560μV)	310μV (3100μV)	400μV (8500μV)
OPAx376	5.2μV (35μV)	7μV (125μV)	25μV (1025μV)

Table 3.3: Performance of the power supply of the first iteration of the test PCB. All measurements were done using a Rigol MSO1074 70MHz oscilloscope and calibrated 150MHz 10x probes. The resolution did not allow measurements below 4mV.

Voltage rail	Ripple+noise	Actual output voltage
0V (test)	<4mVpp	<500μV
5V	<4mVpp	4.97V
5VA	<4mVpp	4.97V
2V5A	<4mVpp	2.50V

3.3. Design of the power stage

The circuit needs multiple sources; one low noise 5V source for the analog amplifier and the ADC, and one low noise 2.5V source for the bias of the sensor.

To realise these loose requirements, two low-noise low-dropout regulators (LDOs) were used to generate the 2.5V and 5V rails. LDOs are linear regulators so they have very low output ripple compared to the buck converter currently used by Momo Medical to generate the 5V. The downside of a linear regulator is that all excess energy is dissipated in heat, which can be calculated with equation 3.10. In this equation, the quiescent current is negligible. Luckily, because the ADC and op-amps only use a few milliamps, the dissipated power is very low (<5mW) and thus the LDOs do not require extra cooling. Both LDOs are able to provide 150mA.

For the separation between the digital and the analog voltage rails some ferrite beads are used, these reduce any remaining high frequency noise from the LDO and ADC.

$$P_{loss} = (V_{in} - V_{out}) \cdot I_{out} \quad (3.10)$$

Results

An overview of the performance of the power supply can be seen in table 3.3. The ripple+noise measured was too low to measure with the oscilloscope used. The output voltages are all within spec (1%).

3.4. Shielding

Because the source impedance is so high, the signal power will be very low and any electromagnetic interference (EMI) will have a high impact on the signal-to-noise ratio. This is why in the sensor plate of Momo Medical two grounded aluminium plates are placed below and on top of the PCBs and sensors. In the test setup, this would be very inconvenient. So in the first PCB, only an EMI shield was placed on the amplifier to keep the sensor exposed. Unfortunately, the sensor still received too much EMI, so in the second iteration a larger shield was selected to encapsulate the entire sensor and the amplifier.

The shields used were the BMI-S-202 and BMI-S-206 of Laird Technologies. These shields have the advantage of consisting of two pieces, the frame and the can, so the components under the shield can be inspected and reworked (see figure 3.11). Another advantage of the BMI-S-2 series is the material thickness, the can is only 0.20mm thick [?], so it bends easily and transfers the force to the sensor.

3.5. Mechanical setup of the sensor

In the first iteration of the board, the sensors were unshielded and exposed on the board, like the PVDF sensor in figure 3.12. When placed under the mattress, the sensors were in direct contact with the mattress.

In the second iteration of the board, the sensors were fixed in a mechanical setup under the EMI shield. The top of the EMI shield is made of a thin plate of metal (0.20mm thick [?]) and bends easily, transferring the force through the pucks to the sensors. The metal also doesn't deform permanently with the force applied through the mattress and bends back. The PZT sensor was setup with large hard pucks, focussing the force in the compression of the sensor, see figure 3.15. The PVDF sensor was setup with a puck placed under the end of the sensor, and two pucks on the shield bending the sensor when force is applied, see figure 3.14. A photo of the setup can be seen in figure 3.13.

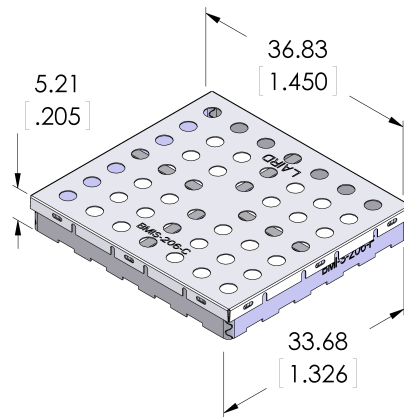


Figure 3.11: The Laird BMI-S-206 EMI shield, which consists of the BMI-S-206-C (can) and the BMI-S-206-F (frame).

Source: Laird Technologies 2018

In both PCBs, the sensor distance was the same as in the board of Momo Medical, which is 200mm from centre to centre.

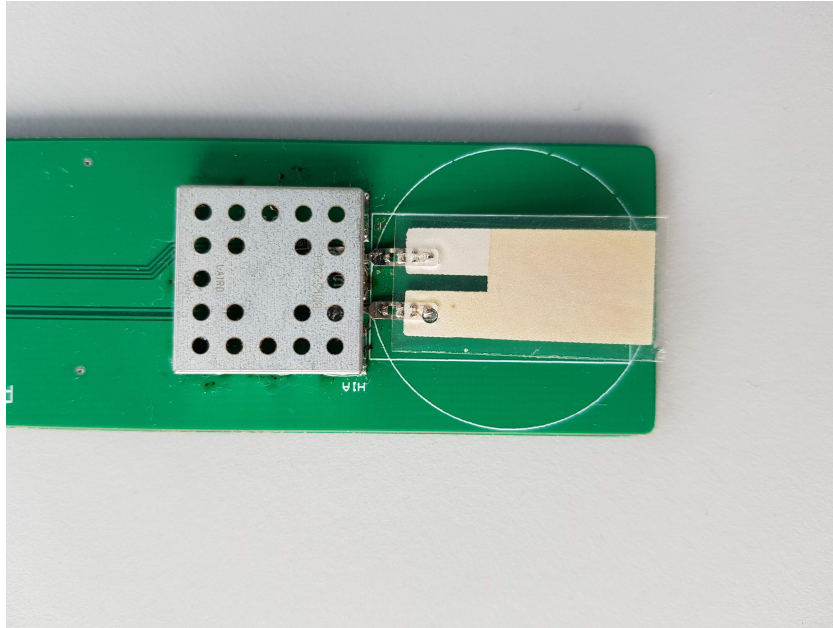


Figure 3.12: Photo of the mechanical setup of the PVDF sensor in the first iteration of the PCB. The sensors would make direct contact with the mattress when placed under it. The EMI shield only covers the amplifier.

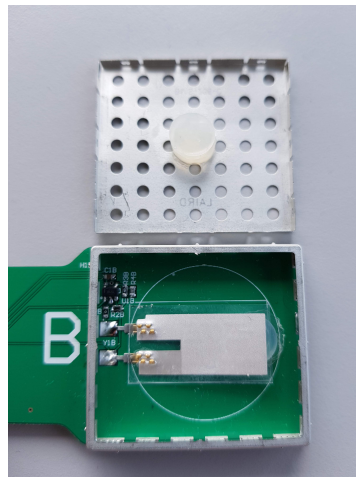


Figure 3.13: Photo of the mechanical setup of the PVDF sensor in the second iteration of the PCB. The top of the EMI shield is detached from the frame and placed upside down above the board. The two white silicon pucks are glued to the EMI shield. The sensors are placed in setup where the force gets transferred through the top of the EMI shield into the sensor. The EMI shield covers the amplifier and the sensor.

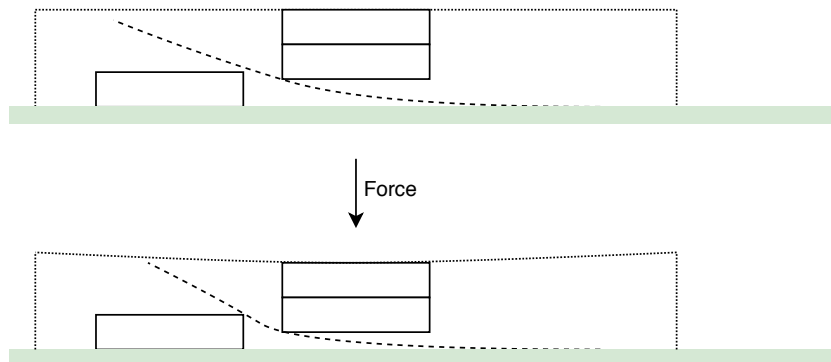


Figure 3.14: Sideview of the mechanical setup of the PVDF sensor. The sensor is represented by the curved dashed line, the silicon pucks are represented by the white rectangles, the dotted line represents the EMI shield. When force is applied to the top of the EMI shield, the top bends and pushes the pucks onto the PVDF sensor, causing it to bend more.

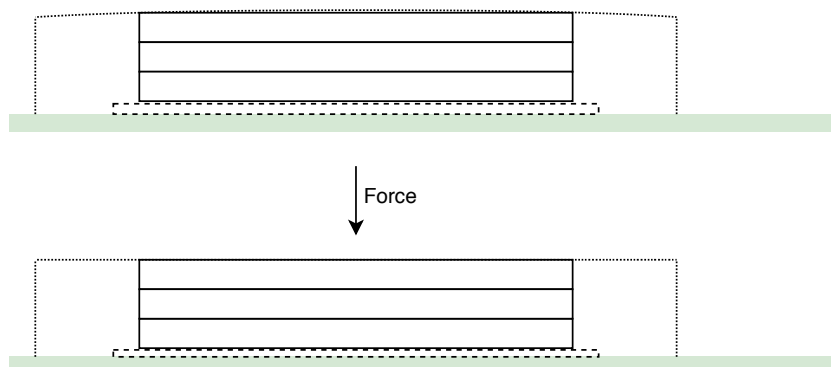


Figure 3.15: Sideview of the mechanical setup of the PZT sensor. The sensor is represented by the curved dashed line, the plastic pucks are represented by the white rectangles, the dotted line represents the EMI shield. When force is applied to the top of the EMI shield, the top bends and pushes the pucks onto the PZT sensor.

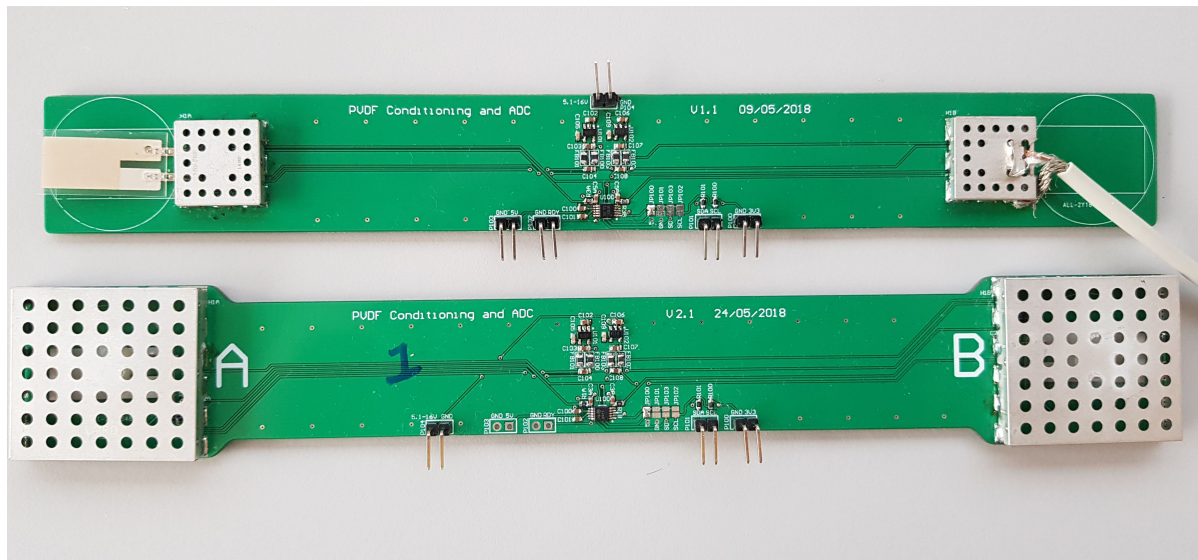


Figure 3.16: The populated printed circuit boards. The first iteration on top (version 1.1) and the second iteration on the below (version 2.1). The first iteration has been altered by Momo Medical for testing purposes (cable on the right side).

3.6. PCB layout

The printed circuit board was designed in Altium's CircuitMaker. CircuitMaker is a free, open-source hardware PCB design platform and is currently used by Momo Medical. In the PCB layout, care was taken to minimise noise. A few features of both iterations of the PCB include:

- The amplifier is placed as close to sensor as possible
- The low-pass filter is placed as close as possible to the ADC
- Ground plane on the bottom layer is as uninterrupted as possible (traces running on the bottom layer are kept short)
- Vias under the shield ensure a complete isolation of external noise and a low impedance connection to the ground plane
- Vias between the ground plane on the top layer and the ground plane on the bottom layer are distributed across the board to minimise the impedance between the planes.
- Decoupling capacitors are placed close to the ADC and op-amp
- All passive components were selected to be 0603 (1608 metric) size. This size is still reasonably easy to solder and rework by hand, and still retains a small footprint.

The changes in the second iteration include moving the connectors to one side of the pcb and changing the form factor to accommodate for the new EMI shield.

A photo of the populated PCBs can be seen in figure 3.16. The first iteration has already been used by Momo Medical to test mechanical setups of sensors. The schematics of the first iteration can be seen in appendix C.1 (ADC stage) C.2 (amplifier stage) and C.3 (power stage). A 3D model can be seen in appendix C.4 and a view from CircuitMaker in appendix C.5. The schematics of the second iteration can be seen in appendix C.6 (ADC stage) C.7 (amplifier stage) and C.8 (power stage). A 3D model can be seen in appendix C.9 and a view from CircuitMaker in appendix C.10.

4

Results

4.1. Determining bandwidth of human bio-signals

In order to be able to determine the performance of the sensors in measuring human bio-signals the bandwidth of these signals needed to be determined. This was done with a test set-up with the least amount of noise. The sensor was shielded and the frequency spectrum was determined with Welch's power spectral density estimate to reduce noise even further. Welch's power spectral density estimate splits the signal up into multiple segments, computes the Fast Fourier Transform (FFT) of these segments and creates an average power spectral density (PSD) of these segments. The bandwidth was determined by looking where the integrated power (up until that frequency) was more than 0.5% of the total power, the lower limit, and where the integrated power was more than 99.5% of the total power, the upper limit. This resulted in a bandwidth from 0.015 to 37 Hz as shown in figure 4.1.

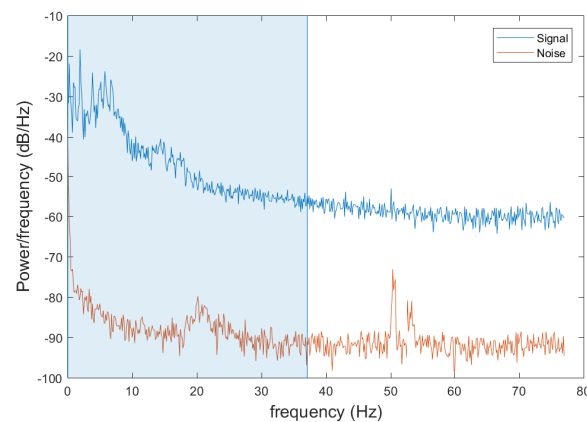


Figure 4.1: Human bio-signals bandwidth estimation. Bandwidth from 0.015 to 37 Hz, highlighted in blue. This plot was generated with script B.6

4.2. Comparing different sensors

To determine the performance of the different test set-ups and sensors the SNR was determined by measuring with and without a patient on the bed, taking the measurement without a patient on the bed as noise.

4.2.1. Existing sensor system with PZT

To be able to determine if the results with new set-ups have improved, the current set-up of Momo Medical was measured. Momo Medical samples the PZT sensors at only 30Hz, the ADC is however capable of a sampling frequency of up to 860 samples/s. The programming on the MCU was changed to

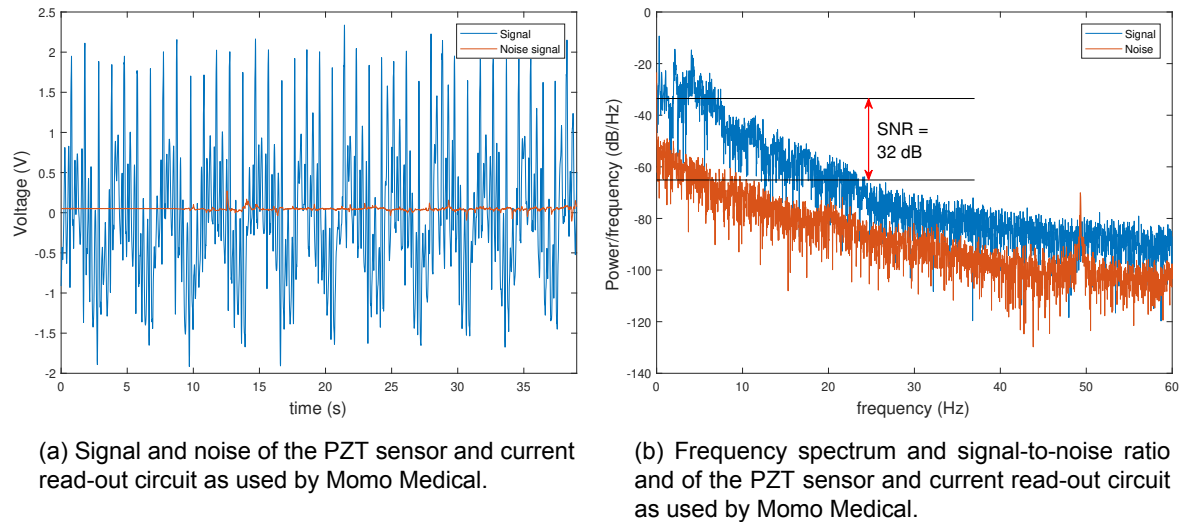


Figure 4.2: Signal to noise analysis of Momo Medical system.

only sample one sensor at a higher sampling frequency (around 630 samples/s), to be able to examine a larger range of frequencies. Figure 4.2 shows the measurements with the Momo Medical sensor set-up. The SNR of the Momo Medical set-up is 32dB.

4.2.2. Comparing PZT and PVDF sensors with first iteration test set-up

The first comparison of the PZT and PVDF sensors was done using the first iteration test set-up, as described in section 3.1.1. As seen from figures 4.3 and 4.4, the SNR of the PZT sensor is 41dB and the SNR of the PVDF sensor is 51dB. It can be seen that the first iteration test set-up does have more noise, especially at 50Hz, but this does not negatively affect the SNR because it is outside of the bandwidth of the human bio-signals. Even though the voltage output of the PZT sensor is higher than the PVDF sensor, the PVDF sensor does have a higher SNR.

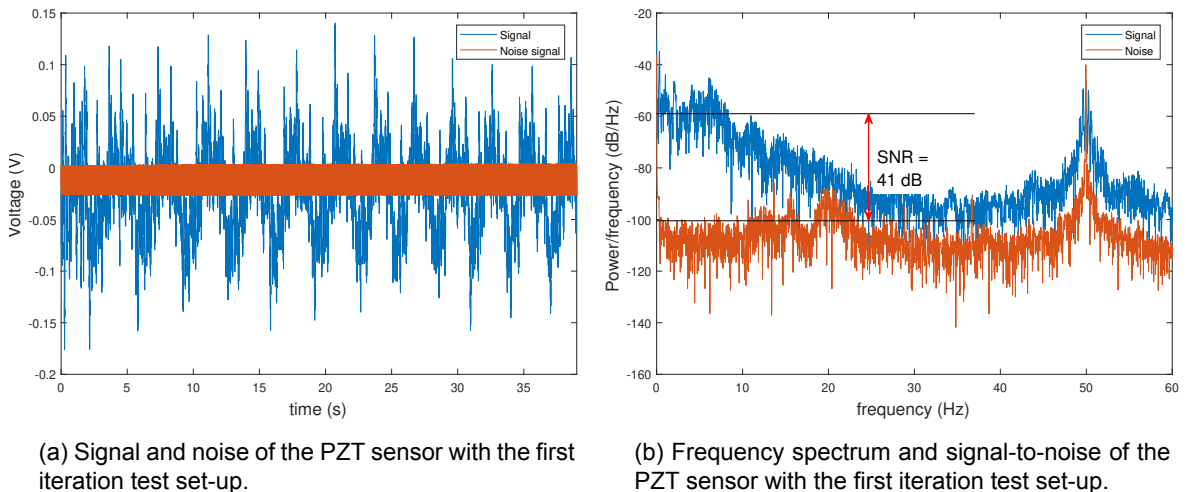


Figure 4.3: Signal to noise analysis of PZT sensor with first iteration test set-up

4.2.3. Comparing PZT and PVDF sensors with second iteration test set-up

A second comparison of the PZT and PVDF sensors was done using the second iteration test set-up as described in section 3.1.1. As seen from figures 4.5 and 4.6, the SNR of the PZT sensor is 22dB and the PVDF sensor is 26dB. It can be seen that the noise at 50Hz is significantly reduced and that the

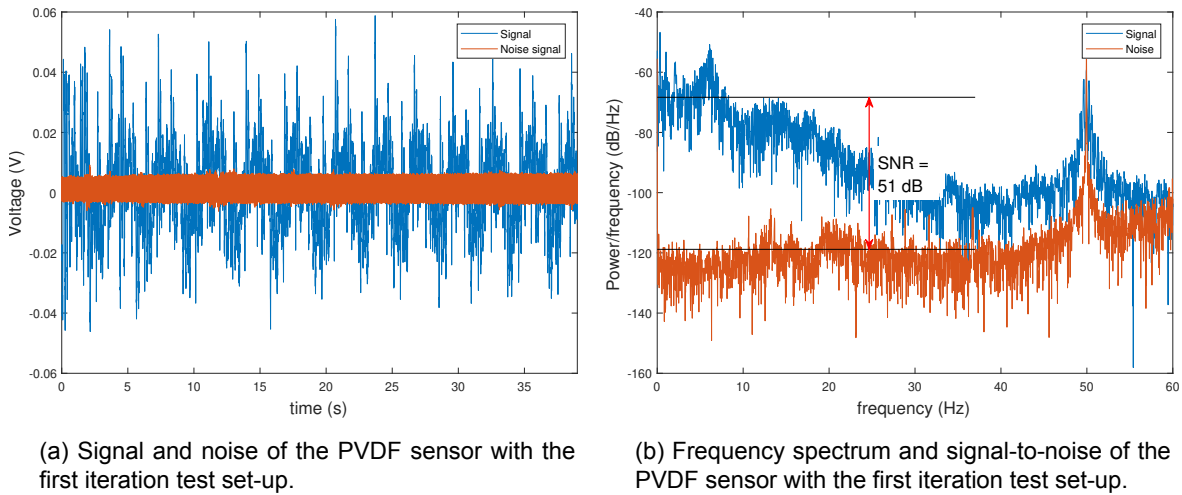


Figure 4.4: Signal to noise analysis of PVDF sensor with first iteration test set-up

overall amount of noise is quite low with the second iteration test set-up, especially the PVDF sensor. The SNR is lower than the first iteration test set-up, what might have caused this will be part of the discussion. The SNR can however still be compared between the two sensors. The PVDF sensor still has a better SNR than the PZT sensor. Looking at the frequency spectrum the PVDF sensor looks to have a lot less noise in the bandwidth of interest, it does however have a lot of noise at low frequencies. This might be due to the drifting offset that can be seen quite clearly in the time domain when looking at a larger time scale. If this can be resolved the PVDF sensor can have an even better SNR, an example of this is shown in figure 4.7 where the measurements were taken with the patient lying still for a long time, because the drift has tapered off.

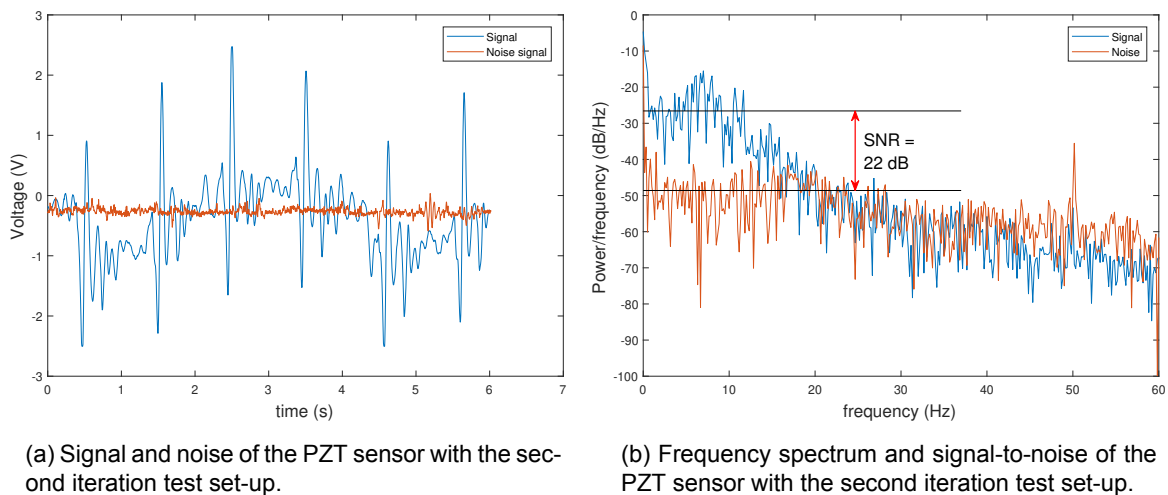


Figure 4.5: Signal to noise analysis of PZT sensor with second iteration test set-up

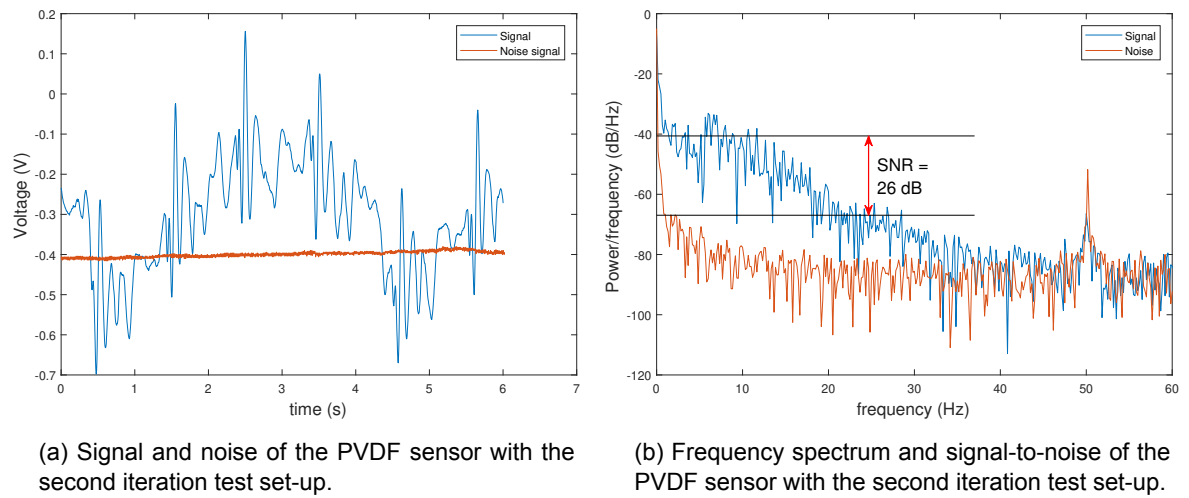


Figure 4.6: Signal to noise analysis of PVDF sensor with second iteration test set-up

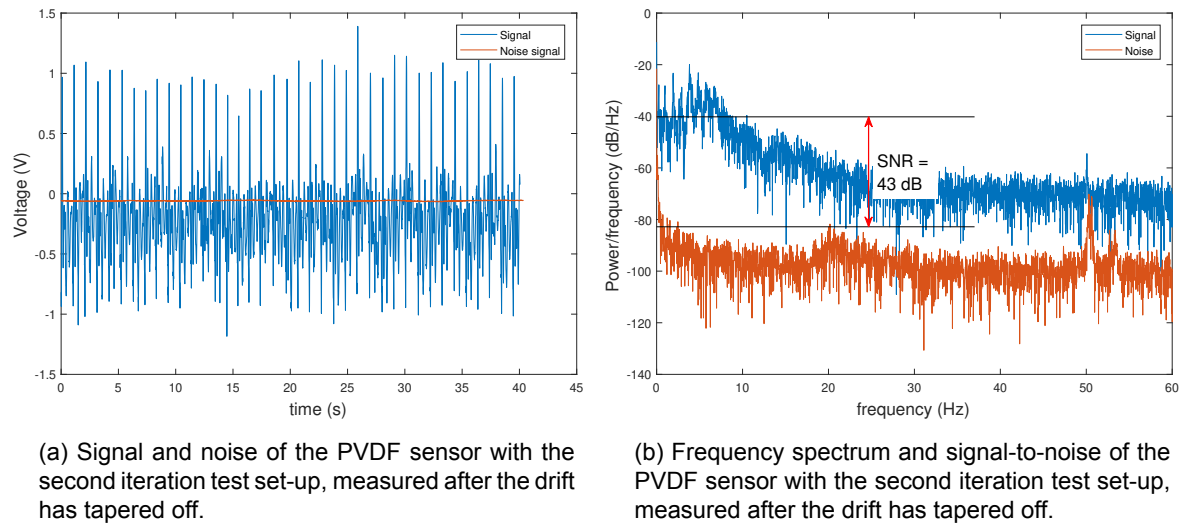


Figure 4.7: Signal to noise analysis of PVDF sensor with second iteration test set-up, measured after the drift has tapered off.

5

Discussion

The mechanical set-up of the PZT in the second iteration test set-up was not optimal, there was a bias force on the sensor and the force was not optimally transferred to the sensor. Using smaller silicon pucks which fit more properly between the sensor and the shield will probably yield better results, as there is less bias force and more deformation of the sensor when force is applied.

The PVDF sensors have lower tolerance than the PZT, but it is not yet clear whether the PVDF sensors will behave the same, because the mechanical set-up might be slightly different for each sensor. This might not have a big effect on the measured signal, but this needs to be measured. It is also not known if the PVDF sensors will keep their properties or whether these properties change under stress of the material. It is known from PZT sensors that they can crack and permanently damage the sensor. If the PVDF sensors are able to handle stresses better this can be an advantage of the PVDF sensors.

The PZT sensor uses lead as one of the elements in the ceramic, even though the European Union (EU) restricts the use of lead in any electronics there is an exemption that allows the use of lead in ceramics [?]. It should however be examined if there are not any stricter rules on medical devices.

There is still a lot of unknowns about what influence the position of the piezoelectric sensors has on the received signal. It is clear that the signal becomes weaker as the sensor is positioned further away from the heart. But a lot more can be determined about the relation between the respiration and heart signal and how it relates to the position of the patient.

In the second iteration of the test set-up the heart and respiration signals are clearly visible, but there is also drift visible. Even though the heart and respiration signals are AC-coupled this is a problem because drift is very low-frequency and especially the respiration signal is also quite low-frequency thus making the respiration signal harder to distinguish.

The results reached in this thesis are quite different from the results Momo Medical reached, especially when it comes to the PVDF sensors. The outcome of this thesis needs to be discussed with Momo Medical, this will give more insight into the use of piezoelectric sensors in measuring human bio-signals. The main difference between the tests performed in this thesis and the sensor plate of Momo Medical is the integration of the mechanical set-up in the sensor plate. In the test set-up the sensors make more direct contact with the mattress, while in the sensor plate the sensors have to be integrated.

5.1. Future work

The drift of the sensors in the second iteration of the test set-up could be reduced or removed. This might be done by lowering the input impedance, thus decreasing the RC time. This will also cause more attenuation because the high-pass filter the sensor forms with the input impedance of the amplifier will be at a higher frequency. This means an optimum can be found, considering the SNR as the main performance factor.

The sensors could be characterised electrically and calibrated in-circuit [?] by developing a new version of the PCB with active circuitry which can generate an electrical impulse on the sensor of which the response can be read out using the ADC.

The measurements comparing the PZT and PVDF could be redone using a better mechanical set-up for the PZT. The PZT can still be a viable option as a sensor if the mechanical set-up is improved.

To improve the reliability of the prediction of the position, it would be useful to determine the optimal positions of the sensors relative to the patient, and the amount of sensors necessary. Profiling BCGs from different patients at different positions could also be very useful in assisting position detection. Signal properties like the ratio between the respiration and BCG could provide insight in the patient's position.

Consistency in the plates and the necessity of calibration can be done by measuring multiple sensors of the same type to determine if they produce the same signal. Also determining the tolerances on the mechanical set-up and how much it influences the signal is important for this purpose. To determine the drift of the properties of a sensor, the sensors should also be stress tested.

To make the production process easier and cheaper, the EMI shielding aluminium plates could be removed if the sensors continue to produce a high SNR. This could be tested by developing a new test PCB with no shielding and active low-pass filters, filtering out the 50Hz noise which is most dominant.

Using the PCBs to test more sensors could also be very viable, as only two types were tested. Sensors like piezoelectric cables or larger piezoelectric films might produce an even better signal.

Eventually reviewing the conclusions and recommendations in this thesis and determining how they can be optimally integrated in the system of Momo Medical would be viable.

6

Conclusions

The thesis presented a clean solution for testing PZT and PVDF sensors, which also has been used by employees of Momo Medical. In the test PCBs, different amplifiers were used, iterating towards a better design producing a higher SNR.

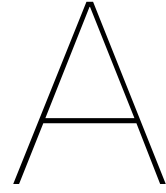
Using the test PCBs, both the PZT and the PVDF sensors produced a better signal than in the sensor plate of Momo Medical, and from both produced clear BCG and respiration signals. These signals have been analysed and processed by group MCU [?]. The FFT of the signals have been analysed and the bandwidth of the signal was determined be from 0.015 to 37Hz.

The PZT and PVDF sensors were compared. In the developed PCB, the SNR of the PVDF sensor was higher than the PZT sensor. It must be noted that the PZT sensor was likely to be in a suboptimal setup in that measurement. However, both sensor have their advantages. The PVDF sensors can also produce a higher signal and thus a higher SNR when put in the right mechanical setup, but this increases the production cost. The PZT sensors are cheaper, but also produce a weaker SNR compared to a mechanically optimised PVDF sensor. PZT sensors do however tend to break very easy, whereas the PVDF sensors were built to bend.

6.1. Recommendations

To make a substantiated choice between the PZT and PVDF sensors, more research should be done. As the quality of the PZT sensor is low, it is recommended to acquire higher quality PZT sensors, which might produce better results.

If Momo Medical decides to choose the PVDF sensor, it is recommended to choose a non-inverting amplifier design, as the gain can be set independently from the input impedance. For the PZT, the non-inverting amplifier did not have any advantages. Whichever amplifier might be chosen, it is recommended to place the amplifier as close to the sensor as possible to minimise the capacitance of the cable and increase the SNR.



Measurement data

Table A.1: Capacitance of 11 PZT sensors. The sensor was placed in an RC low-pass configuration with a 10k 1% resistor. Standard deviation is 1.27nF (5.6%). Signal generated and measured with a Rigol MSO1074 oscilloscope with an accuracy of 1%.

f_{-3dB}	C_p
669Hz	23.4nF
721Hz	21.7nF
670Hz	23.4nF
657Hz	23.9nF
767Hz	20.4nF
669Hz	23.4nF
708Hz	22.1nF
666Hz	23.5nF
694Hz	22.6nF
721Hz	21.7nF
771Hz	20.3nF

Table A.2: Capacitance of 11 PVDF sensors. The sensor was placed in an RC low-pass configuration with a 10k 1% resistor. Standard deviation is 18pF (3.5%). Signal generated and measured with a Rigol MSO1074 oscilloscope with an accuracy of 1%.

f_{-3dB}	C_p
32.9kHz	476pF
32.3kHz	485pF
29.6kHz	530pF
30.8kHz	509pF
31.3kHz	501pF
30.6kHz	512pF
29.1kHz	539pF
30.9kHz	507pF
30.1kHz	521pF
31.0kHz	506pF
31.1kHz	504pF

B

Matlab scripts

Listing B.1: Matlab script used for calculating the capacitance of the PZT sensors and calculating the standard deviation and mean.

```
fc = [  
669,  
721,  
670,  
657,  
767,  
669,  
708,  
666,  
694,  
721,  
771];  
  
R = 10e3;  
Rsg = 50;  
RosC = 1e6;  
Cp = sqrt(2-(1+(R+Rsg)/RosC)^2)/(2*pi*fc*(R+Rsg));  
  
disp(round(Cp*1e9,1));  
  
disp(['Standard deviation of the capacitance of the PZT sensors: ',num2str(std(Cp)*1e9), 'nF ...  
= ',num2str(std(Cp)/mean(Cp)*100), '%']);  
disp(['Mean of the capacitance of the PZT sensors: ',num2str(mean(Cp)*1e9), 'nF']);
```

Listing B.2: Matlab script used for calculating the capacitance of the PVDF sensors and calculating the standard deviation and mean.

```
fc = [  
32.9e3,  
32.3e3,  
29.6e3,  
30.8e3,  
31.3e3,  
30.6e3,  
29.1e3,  
30.9e3,  
30.1e3,  
31.0e3,  
31.1e3];  
  
R = 10e3;  
Rsg = 50;  
RosC = 1e6;  
Cp = sqrt(2-(1+(R+Rsg)/RosC)^2)/(2*pi*fc*(R+Rsg));
```

```

disp(round(Cp*1e12));

disp(['Standard deviation of the capacitance of the PVDF ...
      sensors: ', num2str(std(Cp)*1e12), 'pF = ', num2str(std(Cp)/mean(Cp)*100), '%']);
disp(['Mean of the capacitance of the PVDF sensors: ', num2str(mean(Cp)*1e12), 'pF']);

```

Listing B.3: Matlab script used for calculating the transfer function and plotting the frequency response of the amplifier currently used by Momo Medical

```

clear all
close all

% For the PZT sensors
s = tf('s');
Cp = 22.4e-9;
R1 = 820e3;
R2 = 250e6;
C1 = 62e-12;
R3 = 3e3;
C2 = 4.7e-6;

% Series RC of Cp with R1
Z1 = R1 + 1/(s*Cp);
% Parallel RC of C1 with R2
Z2 = 1/(1/R2 + s*C1);
% R3
Z3 = R3;
% C2
Z4 = 1/(s*C2);

Hamp = -Z2/Z1;
H1pf = Z4/(Z4+Z3);
Hpzt = Hamp*H1pf;
Hpzt_q = 1/Cp*Hamp*H1pf;

% For the PVDF sensors
s = tf('s');
Cp = 508e-12;
R1 = 820e3;
R2 = 250e6;
C1 = 62e-12;
R3 = 3e3;
C2 = 4.7e-6;

% Series RC of Cp with R1
Z1 = R1 + 1/(s*Cp);
% Parallel RC of C1 with R2
Z2 = 1/(1/R2 + s*C1);
% R3
Z3 = R3;
% C2
Z4 = 1/(s*C2);

Hamp = -Z2/Z1;
H1pf = Z4/(Z4+Z3);
Hpvdf = Hamp*H1pf;
Hpvdf_q = 1/Cp*Hamp*H1pf;

p = bodeplot(Hpzt, {10e-1 10e2});
hold on;
bodeplot(Hpvdf, {10e-1 10e2});
opt = getoptions(p);
opt.FreqUnits = 'Hz';
opt.PhaseVisible = 'off';
opt.Title.String = '';
opt.Grid = 'on';
setoptions(p, opt);

axes_handles = findall(gcf, 'type', 'axes');
legend(axes_handles(3), 'PZT', 'PVDF');

```

```

% calculating gain at 0.5Hz
fi = 0.5;
a = 2*pi*fi*1i;
disp(['PZT Gain at ', num2str(fi), 'Hz: ', num2str(20*log10(abs(evalfr(Hpzt,a))))], 'dB');
disp(['PVDF Gain at ', num2str(fi), 'Hz: ', num2str(20*log10(abs(evalfr(Hpvdf,a))))], 'dB');

disp(['PZT poles:']);
pole(Hpzt)./(-2*pi)
disp(['PVDF poles:']);
pole(Hpvdf)./(-2*pi)

```

Listing B.4: Matlab script used for calculating the transfer function and plotting the frequency response of the amplifier of the first iteration of the test PCB

```

clear all
close all

% For the PZT sensors
s = tf('s');
Cp = 22.4e-9;
R1 = 820e3;
R2 = 500e6;
R3 = 100e3;
C1 = 150e-9;

% Series RC of Cp with R1
Z1 = R1 + 1/(s*Cp);
% R2
Z2 = R2;
% R3
Z3 = R3;
% C2
Z4 = 1/(s*C1);

Hamp = -Z2/Z1;
Hlpf = Z4/(Z4+Z3);
Hpzt = Hamp*Hlpf;
Hpzt_q = 1/Cp*Hamp*Hlpf;

% For the PVDF sensors
s = tf('s');
Cp = 508e-12;
R1 = 820e3;
R2 = 500e6;
C1 = 62e-12;
R3 = 100e3;
C2 = 150e-9;

% Series RC of Cp with R1
Z1 = R1 + 1/(s*Cp);
% R2
Z2 = R2;
% R3
Z3 = R3;
% C2
Z4 = 1/(s*C1);

Hamp = -Z2/Z1;
Hlpf = Z4/(Z4+Z3);
Hpvdf = Hamp*Hlpf;
Hpvdf_q = 1/Cp*Hamp*Hlpf;

p = bodeplot(Hpzt,{10e-1 10e2});
hold on;
bodeplot(Hpvdf,{10e-1 10e2});
opt = getoptions(p);
opt.FreqUnits = 'Hz';
opt.PhaseVisible = 'off';
opt.Title.String = '';

```

```

opt.Grid = 'on';
setoptions(p,opt);

axes_handles = findall(gcf, 'type', 'axes');
legend(axes_handles(3), 'PZT', 'PVDF');

% calculating gain at 0.5Hz
fi = 0.5;
a = 2*pi*fi*1i;
disp(['PZT Gain at ', num2str(fi), 'Hz: ', num2str(20*log10(abs(evalfr(Hpzt,a))), 'dB']);
disp(['PVDF Gain at ', num2str(fi), 'Hz: ', num2str(20*log10(abs(evalfr(Hpvdf,a))), 'dB']);

disp(['PZT poles: ']);
pole(Hpzt_q)/(-2*pi)
disp(['PVDF poles: ']);
pole(Hpvdf_q)/(-2*pi)

```

Listing B.5: Matlab script used for calculating the transfer function and plotting the frequency response of the amplifier of the second iteration of the test PCB

```

clear all
close all

% For the pvdf
s = tf('s');
Cp = 508e-12;
R1 = 100e6;
R2 = 499;
R3 = 100e3;
C1 = 150e-9;
R4 = 10e3;

Zp = 1/(s*Cp);
% C2
Z1 = 1/(s*C1);

Hhpf = R1/(Zp+R1);
Hamp = 1+R3/R2;
Hlpf = Z1/(Z1+R4);
Hpvdf = Hhpf*Hamp*Hlpf;
Hpvdf_q = 1/Cp*Hhpf*Hamp*Hlpf;

% For the pzt
s = tf('s');
Cp = 22.4e-9;
R1 = 100e6;
R2 = 499;
R3 = 100e3;
C1 = 150e-9;
R4 = 10e3;

Zp = 1/(s*Cp);
% C2
Z1 = 1/(s*C1);

Hhpf = R1/(Zp+R1);
Hamp = 1+R3/R2;
Hlpf = Z1/(Z1+R4);
Hpzt = Hhpf*Hamp*Hlpf;
Hpzt_q = Hhpf*Hamp*Hlpf;

p = bodeplot(Hpzt,{10e-1 10e2});
hold on;
bodeplot(Hpvdf,{10e-1 10e2});
opt = getoptions(p);
opt.FreqUnits = 'Hz';
opt.PhaseVisible = 'off';
opt.Title.String = '';
opt.Grid = 'on';
setoptions(p,opt);

```

```

axes_handles = findall(gcf, 'type', 'axes');
legend(axes_handles(3), 'PZT', 'PVDF');

% calculating gain at 0.5Hz
fi = 0.5;
a = 2*pi*fi*1i;
disp(['PZT Gain at ', num2str(fi), 'Hz: ', num2str(20*log10(abs(evalfr(Hpzt,a))))], 'dB']);
disp(['PVDF Gain at ', num2str(fi), 'Hz: ', num2str(20*log10(abs(evalfr(Hpvdf,a))))], 'dB']);

disp(['PZT poles:']);
pole(Hpzt)./(-2*pi)
disp(['PVDF poles:']);
pole(Hpvdf)./(-2*pi)

```

Listing B.6: Matlab script used for determining the bandwidth of the human bio-signals

```

% read in data
filename = 'data\calibration_test\patient_on_bed_1.1\output.csv';
val = csvread(filename, 1, 0);
t = val(:,1);
elec = val(:,2);

% calculate sample frequency
dt = mean(diff(t));
Fs = round(1/dt);

filename = 'data\calibration_test\zero_measurement\output.csv';
val = csvread(filename, 1, 0);
t_n = val(:,1);
elec_n = val(:,2);

resp_rate = 15; % per minute
M = 10; % number of respirations to capture
rep_period = 60/resp_rate;
sample_len = M*rep_period;
L = sample_len*Fs;
start = find(t>400,1);
t_selc = t(start:start+L-1);
elec_selc = elec(start:start+L-1,:);
start = find(t_n>1210,1);
t_n_selc = t_n(start:start+L-1);
elec_n_selc = elec_n(start:start+L-1,:);

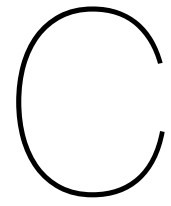
% size of FFT pwelch will use
NFFT = 1200;
SegmentLength = NFFT;

h = figure;
h.Position(3:4) = [720 480];
[P,~] = pwelch(elec_selc, ones(SegmentLength,1), 0, NFFT, Fs, 'power');
[P_N,F] = pwelch(elec_n_selc, ones(SegmentLength,1), 0, NFFT, Fs, 'power');
plot(F, pow2db(P));
hold on;
plot(F, pow2db(P_N));
hold off;
xlabel("frequency (Hz)", 'FontSize', 14);
ylabel("Power/frequency (dB/Hz)", 'FontSize', 14);

total_power = sum(P);
% find bandwidth where power is greater than 0.5 percent
% and smaller than 99.5 percent
I1 = find(cumsum(P)>(0.005*total_power), 1);
I2 = find(cumsum(P)>(0.995*total_power), 1);
Fmin = F(I1);
Fmax = F(I2);
line([Fmin Fmin], ylim);
line([Fmax Fmax], ylim);
y_val = ylim;
patch('XData', [Fmin Fmax Fmax Fmin], ...

```

```
'YData', [y_val(1) y_val(1) y_val(2) y_val(2)], ...  
'FaceColor', [0 0.447 0.741], ...  
'FaceAlpha', 0.125, ...  
'EdgeColor', 'none');  
legend(["Signal" "Noise"]);
```



Printed circuit board design

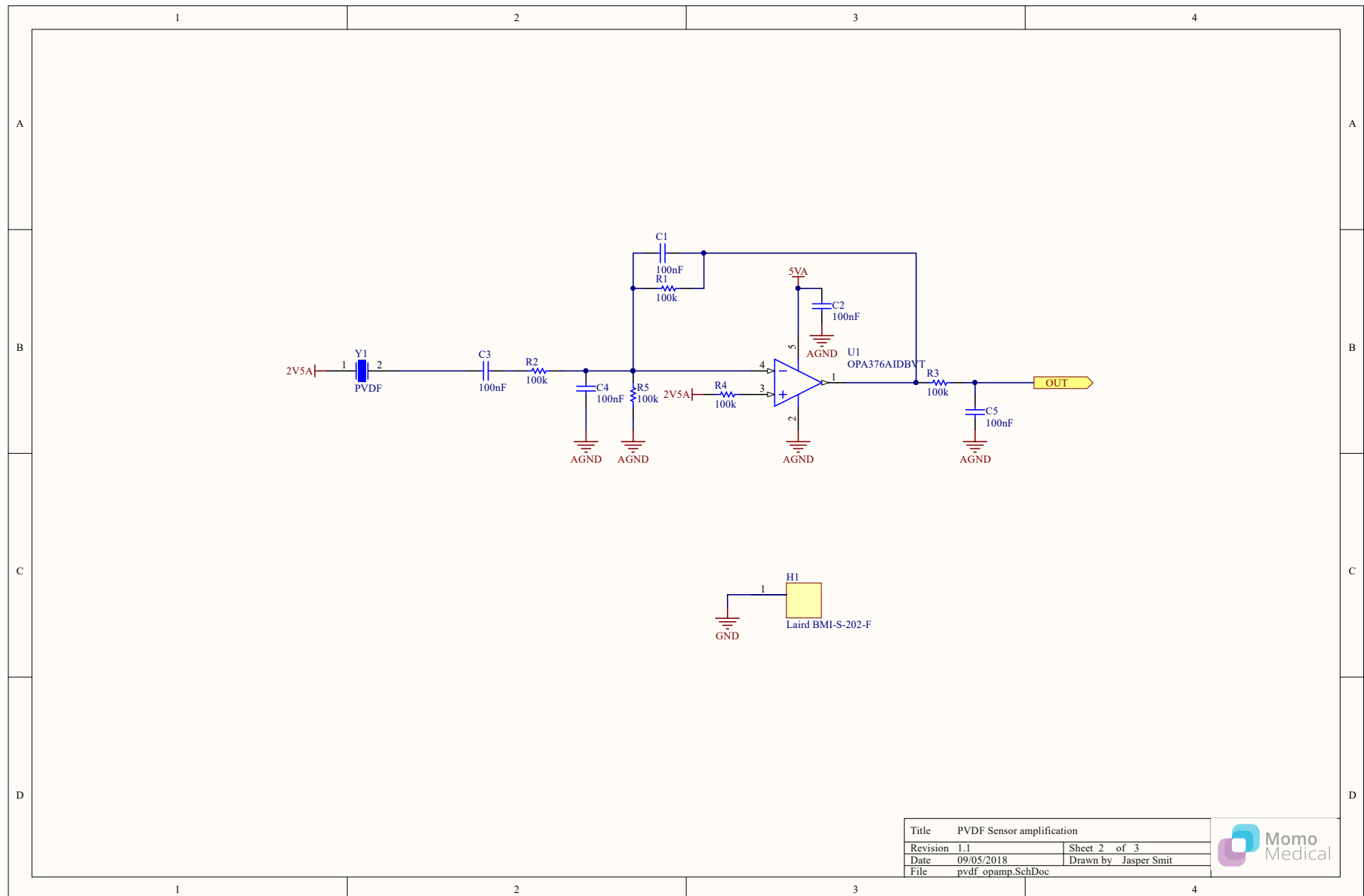


Figure C.2: Schematic of the amplifier stage of the first iteration of the board. C_2 was shorted, R_2 was populated with a 820k Ω resistor, C_5 was populated with a 150nF capacitor. C_1 , C_4 , R_4 , and R_5 were not populated.

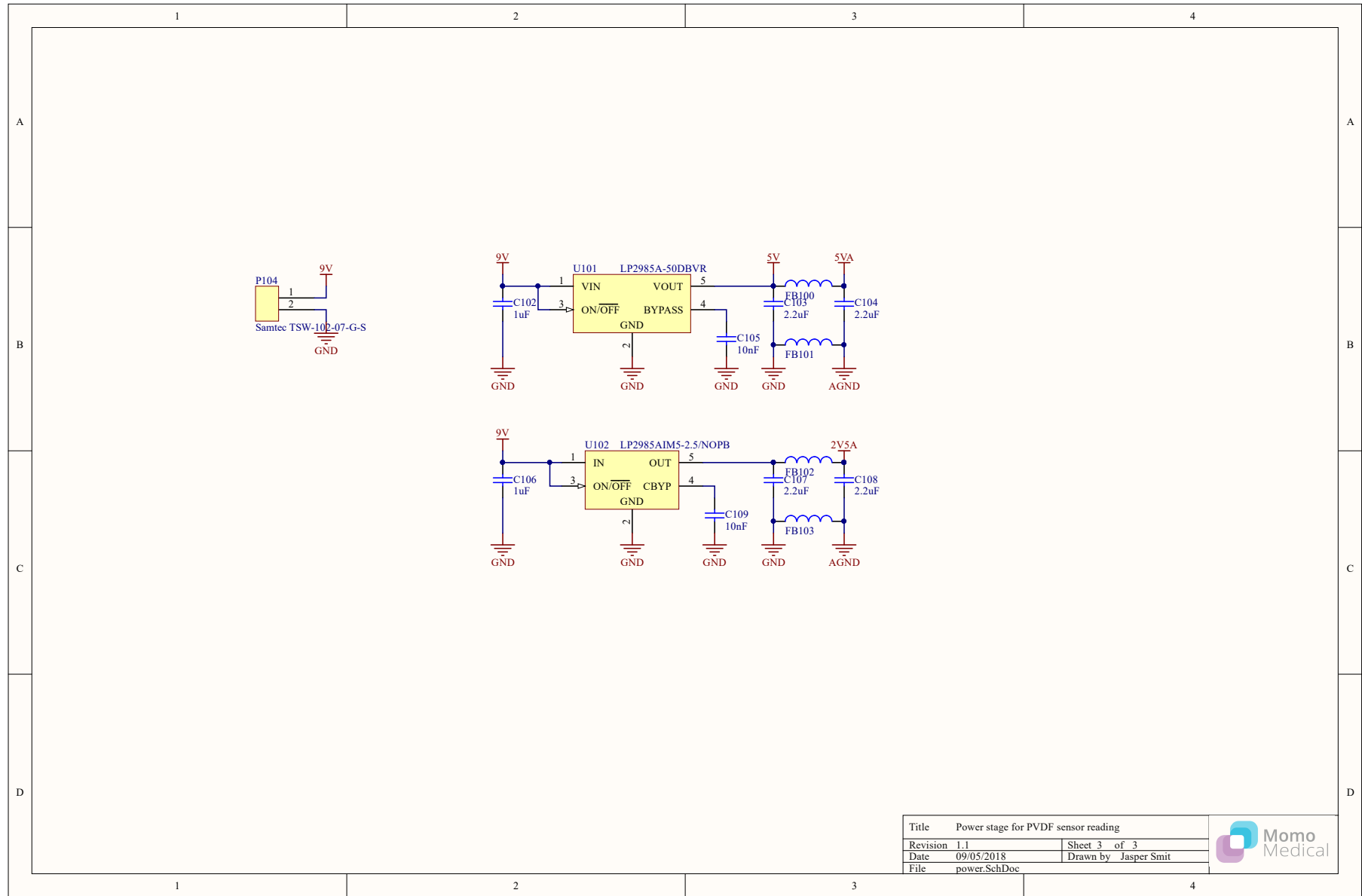


Figure C.3: Schematic of the power stage of the first iteration of the board.

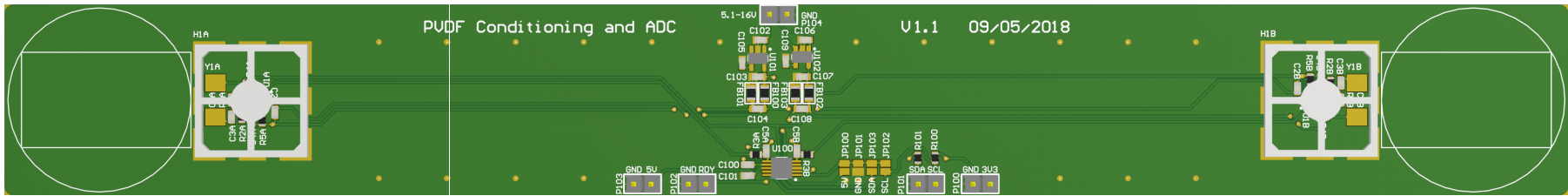


Figure C.4: 3D render of the first iteration of the board. The big rectangles and circles indicate the position for the sensors.

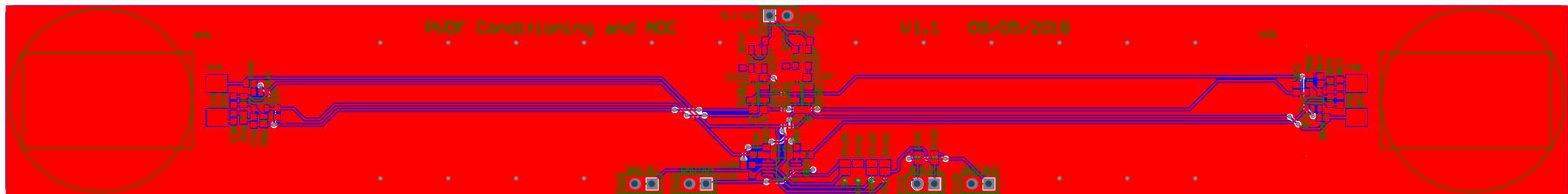


Figure C.5: Design view of the first iteration of the board. The red layer is the top layer, the blue layer is the bottom layer. The big rectangles and circles indicate the position for the sensors.

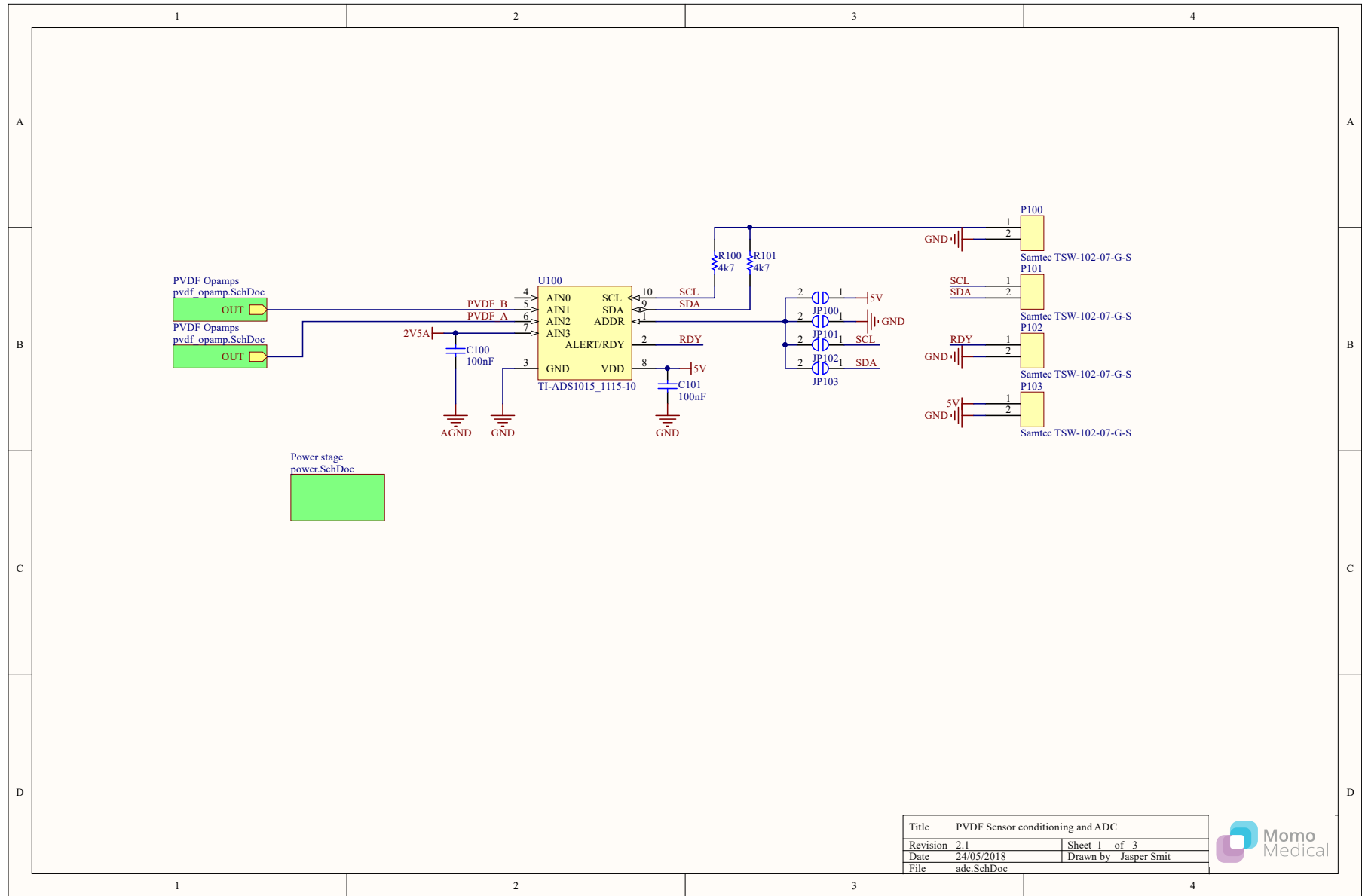


Figure C.6: Schematic of the ADC stage of the second iteration of the board.

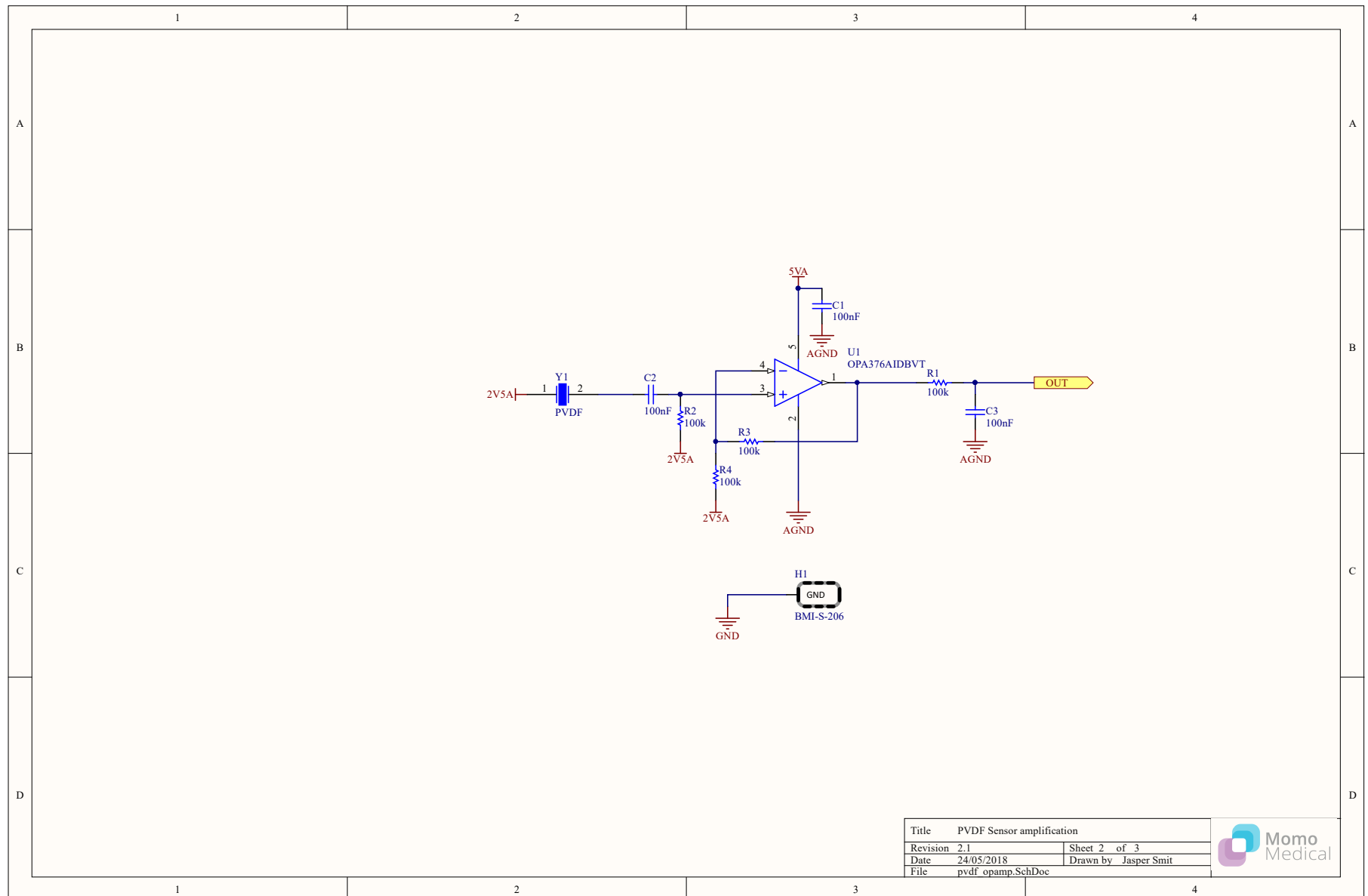


Figure C.7: Schematic of the amplifier stage of the second iteration of the board. C_2 was shorted, R_2 was populated with a 100MΩ resistor, C_1 was populated with a 150nF capacitor, R_3 was populated with a 100kΩ resistor, and R_4 was populated with a 499Ω resistor.

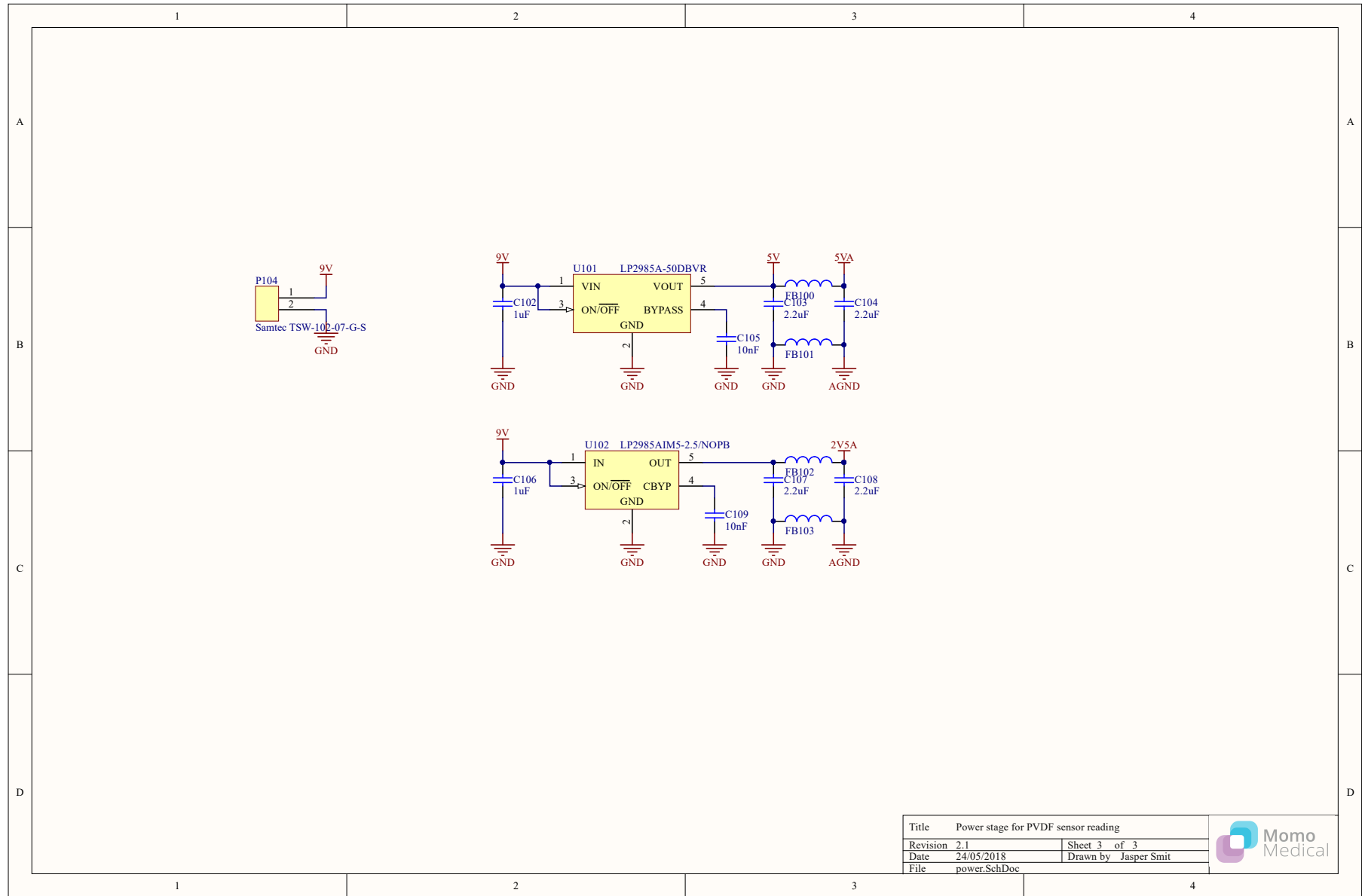


Figure C.8: Schematic of the power stage of the second iteration of the board.

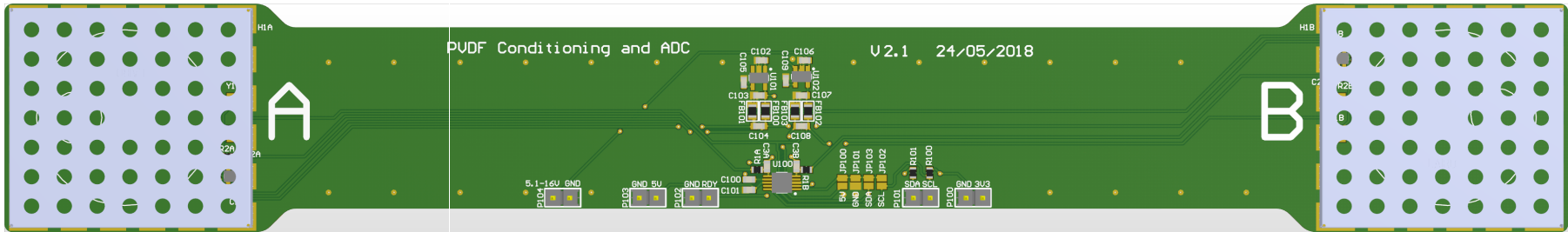


Figure C.9: 3D render of the second iteration of the board. The big rectangles and circles indicate the position for the sensors.

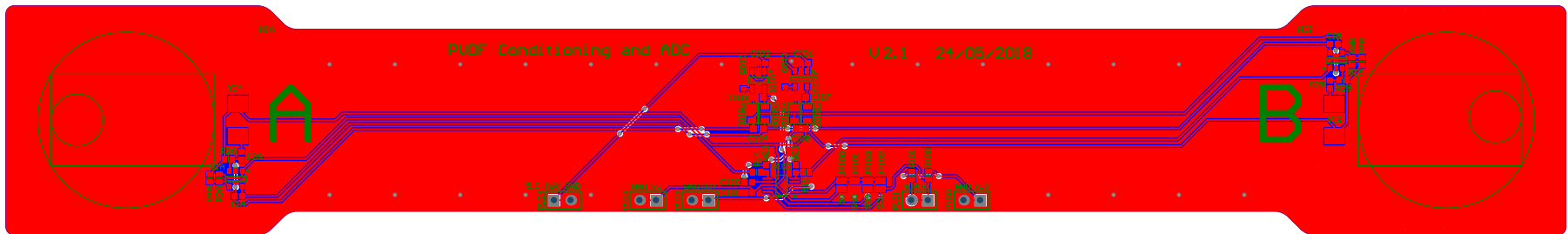


Figure C.10: Design view of the second iteration of the board. The red layer is the top layer, the blue layer is the bottom layer. The big rectangles and circles indicate the position for the sensors.